Design and Analysis of Wide Band, Triple Band and Dielectric Resonator Antenna for Terahertz Applications

A report submitted in fulfillment for the award of the degree of

Integrated Post Graduate in Information Technology

Bachelors of Technology Project

By

Nihit Moolaney (2021IMT-069)

Abhijeet Singh (2021IMT-002)

Adarsh Gautam (2021IMT-003)

Kumar Gaurav (2021IMT-057)

Under the Supervision of

Dr. Pinku Ranjan

Department of Electrical and Electronics

&

Dr. Sunil Kumar

Department of Information Technology

ABV-INDIAN INSTITUTE OF INFORMATION TECHNOLOGY AND MANAGEMENT GWALIOR

GWALIOR, INDIA

DECLARATION

We hereby certify that the work, which is being presented in the report/thesis, entitled **Design and Analysis of Wide Band, Triple Band and Dielectric Resonator Antenna for Terahertz Applications**, in fulfillment of the requirement for the award of the degree of **Integrated Post Graduate - Master of Technology in Information Technology** and submitted to the institution is an authentic record of our own work carried out during the period May-2024 to July-2024 under the supervision of **Dr. Pinku Ranjan and Dr. Sunil Kumar**. We have also cited the reference about the text(s)/figure(s)/table(s) from where they have been taken.

Dated: **Signature of the candidate**

This is to certify that the above statement made by the candidates is correct to the best of my knowledge.

Dated: **Signature of supervisor**

Signature of supervisor

Acknowledgements

We are highly indebted to Dr. Pinku Ranjan and Dr. Sunil Kumar , for his esteemed mentorship, and for allowing us to freely explore and experiment with various ideas in the course of making this project a reality. The leeway we were given went a long way towards helping cultivate a genuine hunger for knowledge and keeping up the motivation to achieve the best possible outcome. We can genuinely say that this Bachelor's Thesis Project (BTP) made us explore many areas of interest that are new to us, and kindled an interest to further follow up on some of those areas. Moreover, the semi-successful completion of this project has brought with it great satisfaction and more importantly, confidence in our ability to produce more high-quality non-trivial systems that can make a difference in the real-world. We would like to sincerely express my gratitude to this prestigious institution for providing us with the opportunity to pursue this BTP. It is an honor to be able to work on such an important academic project under the guidance and support we are provided with. We are grateful for the resources and facilities provided by this institution, which have been instrumental in enabling us to conduct our research and complete this project. Moreover, we deeply appreciate the efforts of our professors in mentoring and fairly evaluating our works.

Nihit Moolaney

Abhijeet Singh

Adarsh Gautam

Kumar Gaurav

Abstract

The demand for rapid communication has driven the development of THz antennas capable of delivering high data rates, speeds, and frequencies. Nevertheless, the limited availability of antenna systems that function effectively in the terahertz band remains a significant barrier to the practical implementation of terahertz devices. In this project, a THz antenna is designed utilizing graphene metamaterial. The proposed antenna employs a microstrip patch on a polyimide substrate with dimensions of 40x40 μm^2 and 50x40 μm^2 ($\epsilon_r = 3.5$), and a copper ground layer with a thickness of 0.035 μm. The conducting elements and feedline are composed of graphene metamaterial shaped as a rectangular ring. This design achieves a maximum gain of 6.59 dB. The antenna configuration is refined using structural parametric optimization, where various geometrical parameters are adjusted. The triple wideband response of the proposed antenna makes it highly suitable for high-speed communication applications.

Keywords: Terahertz, Wide band, Antenna, Graphene, CST Studio, Metamaterials

Contents

List of Figures

List of Tables

1

Introduction

This section presents introduction in the area of antenna design, Terahertz spectrum and Graphene Metamaterials that is pertinent. This section is followed by the Literature Review section.

1.1 Introduction

The rapid evolution of wireless technology has driven the exploration of higher frequency ranges, with particular emphasis on the terahertz (THz) band (0.1–10 THz). This frequency range is increasingly recognized as a promising frontier for future wireless communication systems due to its capability to offer significantly wider bandwidth and much higher data transfer rates than the conventional microwave and millimeter-wave bands. The THz band is not only being viewed as the next step in the evolution of wireless communication but also holds immense potential across various applications, including high-speed secure data transmission, Internet of Things (IoT) devices, biomedical imaging, spectroscopy, sensing, and even in spacecraft communication systems. The distinctive advantages of THz waves, such as ultra-low latency, reduced energy consumption, and their ability to support a large number of high-capacity channels, make them an ideal candidate for addressing the growing demand for faster and more efficient wireless networks.

As THz wireless systems advance, the need for sophisticated antenna designs becomes more pressing. Antennas operating at THz frequencies must deliver not only high gain and radiation efficiency but also features like tunability, reconfigurability, and compactness to meet the varied demands of modern applications. Recent research has classified THz antennas into three main categories based on the materials used: metallic, dielectric, and graphene-based antennas, each offering its own set of benefits and challenges.

Metallic antennas, while popular in microwave and millimeter-wave applications, suffer from significant efficiency losses at THz frequencies. This is due to the high imaginary component of their permittivity, which reduces conductivity and increases the risk of oxidation. On the other hand, graphene-based antennas, which are valued for their reconfigurable frequency responses and tunable radiation characteristics, face their own challenges. They tend to be inefficient for long-distance communication due to substantial absorption losses at the graphene-air interface.

A growing area of interest in THz antenna development is the creation of antennas

with multiplexing capabilities. These antennas, often called self-diplexing antennas, can transmit and receive multiple signals across different frequencies using a single antenna, eliminating the need for external diplexers in radar systems and other applications. The use of graphene and dielectric materials in these antennas shows promise for achieving the required reconfigurability and efficiency, making them suitable for advanced THz applications like imaging, sensing, and secure communication.

In summary, the research and development of THz antennas are crucial for the next generation of wireless technologies. These antennas must excel in gain, efficiency, tunability, and compactness. By integrating innovative materials like graphene with traditional dielectric and metallic structures, researchers are working to overcome the limitations of current designs. The progress in developing tunable and reconfigurable THz antennas is set to be a key factor in realizing high-speed, high-capacity wireless networks. As these technologies continue to evolve, they have the potential to revolutionize various sectors, from telecommunications and defense to healthcare, by enabling faster, more reliable, and versatile wireless communication systems.

1.2 Terahertz Spectrum

Terahertz electromagnetic waves are generally defined by their wavelength range of 0.03-3 mm and a frequency range of 0.1-10 THz [1] (1 THz = 10^{12} Hz). According to the IEEE standard, THz waves are located between 0.3 and 10 THz. This range of the spectrum is situated between the microwave and infrared regions, as illustrated in Figure 1.

THz waves offer several key benefits:

- **Minimal Harm:** THz waves have much lower photon energy compared to X-rays—about one part per million—making them ideal for medical applications, such as skin cancer detection, where they can be used safely without damaging living tissues.

- **High Spectral Precision:** The THz range is vital for detecting hazardous sub-

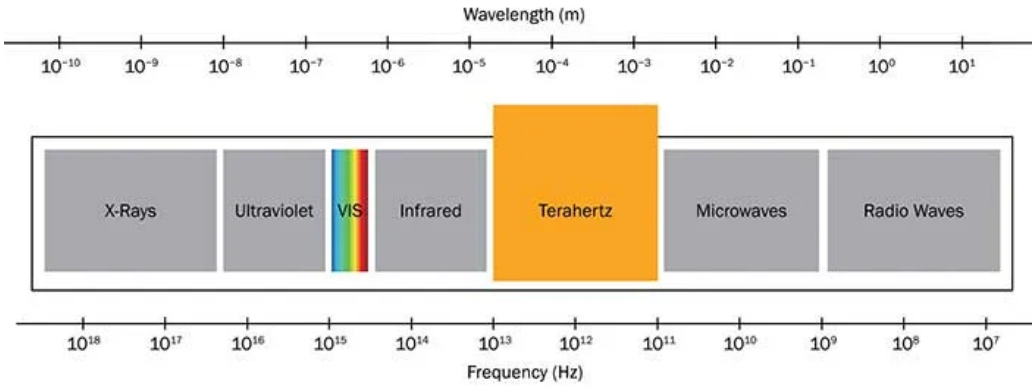

Figure 1.1: The Terahertz region in the electromagnetic spectrum lies between the Infrared and Microwave regions.

stances, as many large molecules have unique spectral signatures in this band. This makes THz waves particularly useful for identifying chemicals, explosives, weapons, and even viruses.

- **Imaging Ability:** THz waves can penetrate certain materials, such as non-polar or non-metallic substances, to create detailed images of objects that are typically opaque. This capability is especially valuable in applications like airport security scanners.

- **Wide Frequency Range:** THz waves occupy the highest frequency band in the electromagnetic spectrum. When used for communication, they have the potential to greatly increase data transmission speeds, reaching up to terabits per second (Tbps).

In summary, although THz waves have seen significant progress in sensing applications, the development of THz antennas is still in its early stages. Given the limited spectrum, antennas are being designed for higher frequencies. THz antennas offer much wider bandwidths than traditional ones, enabling faster data transfer. The growing demand for high-bandwidth, high-gain THz antennas is driving research into metamaterials, especially graphene, to enhance these properties.

However, to fully utilize the Terahertz (THz) band, several challenges need

to be tackled in communication and sensing applications:

- **Signal Loss:** As frequencies move beyond 30 GHz into the terahertz range, challenges like signal attenuation, air absorption, and free space path loss become more significant. Taller antennas with improved directivity can help reduce these losses, but the narrower beam widths present challenges for signal tracking and acquisition, particularly in mobile contexts [2].

- **Efficient Spectrum Use:** The large bandwidth available in the terahertz range is ideal for high-speed data transmission. However, ensuring spectral efficiency is difficult due to interference from other wireless systems operating in nearby frequency bands. Advanced modulation and coding techniques are essential to reduce interference and optimize data throughput.

- **Component Development:** Developing reliable and cost-effective terahertz components—like sources, detectors, amplifiers, and antennas—remains a major challenge. These components must work efficiently at terahertz frequencies while also meeting requirements for power consumption, size, and integration.

- **Security and Privacy:** The unique characteristics of THz waves open up new possibilities for security screening, imaging, and spectroscopy. However, ensuring the security and privacy of transmitted data is critical, necessitating the development of secure encryption and authentication methods specifically for THz communication.

- **Regulatory and Safety Standards:** As with any new technology, establishing regulatory and safety standards is crucial for the widespread adoption of THz-based systems. Setting guidelines for radiation exposure limits, interference mitigation, and spectrum allocation will be essential to ensure these technologies are deployed safely and responsibly [3].

2

Literature Review

In this section we cover an in-depth analysis of the relevant research papers and articles that have played a crucial role in building the foundation of the project.

2.1 Background

The terahertz (THz) spectrum, which lies between the microwave and infrared bands and covers frequencies from 0.1 to 10 THz, is gaining attention for its promising applications. Recently, the THz spectrum has emerged as a key area of interest, particularly in high-speed data transmission for Internet of Things (IoT) applications. Due to its unique properties, such as the potential for high-bandwidth communication and the ability to penetrate various materials, the THz spectrum is seen as a compelling solution to meet the growing demands of IoT networks. As research and technology continue to advance, the exploration of the terahertz band for improved data transmission capabilities shows great potential to revolutionize communication networks and drive IoT innovations [4].

2.2 Key Related Research

The push for high-performance metrics in miniaturized THz antennas has brought about both challenges and opportunities, which are expected to propel antenna technology forward. Some notable THz antenna designs include on-chip antennas [5], metamaterial-loaded antennas [6], and substrate integrated waveguide (SIW) antennas [7], among others. Despite their innovative designs, these THz antenna structures encounter issues such as larger physical sizes, higher production costs, difficulties in integrating with planar circuits, and complex design requirements.

Conversely, microstrip antennas, with their advantages such as low cost, simple design, lightweight, and compact size, have gained attention for terahertz short-range wireless applications as planar technology continues to evolve. Despite their numerous advantages, their limited bandwidth restricts their use across the wide THz spectrum. The focus is therefore on developing antennas that are wideband, compact, and less bulky, capable of handling a variety of THz frequency range applications.

In [8], the authors propose a modification to the rectangular patch microstrip array antenna design with an inset line and a rectangular slot to image thicker breast tissue.

The antenna operates at 0.312 THz, with a bandwidth of 22.68 GHz, a gain of 5.6 dB, and beamwidths of 86.5 degrees horizontally and 47.1 degrees vertically.

In [9], a conductor-backed coplanar waveguide (CPW) interdigital capacitor-based microstrip patch antenna is proposed, which radiates across a bandwidth of 280 GHz within the frequency range of 5.28 THz to 5.56 THz, achieving a realized gain of nearly 10 dB at the resonant frequency of 5.41 THz. The antenna utilizes a silicon dioxide substrate, with gold as the ground and radiating elements. The proposed antenna shows potential for medical applications, including explosives detection and the identification of tumors and malignant cells.

In [10], researchers developed and analyzed five terahertz microstrip patch antennas within the 0.5 to 0.8 THz frequency range, using a modified photonic bandgap substrate. Among these, the second antenna configuration yielded the best results, with a very low return loss of -83.73 dB, a bandwidth reaching 230 GHz, a radiation efficiency of 90.84%, and a gain of 9.19 dB.

In [11], a high-performance THz microstrip patch antenna is designed using a photonic bandgap and a defected ground structure. The proposed antenna operates at a frequency of 0.690 THz, with a near-unity VSWR of up to 1.0015, a return loss of -64.16 dBi, a gain of 6.793 dBi, and a directivity of 6.914 dBi. The antenna's bandwidth is 26.7 GHz.

In [12], an octagonal shorted annular ring (OSAR) antenna array is presented, based on a 130-nm SiGe substrate. The design and fabrication of the 1 x 2 OSAR antenna array cover a substrate area of 550 x 1100 μm^2. The observed -10 dB impedance bandwidth exceeds 17 GHz (303-320 GHz). The proposed on-chip antenna array achieves a predicted radiation efficiency of 38% and a measured gain of 4.1 dBi at 320 GHz.

In [13], the authors present a novel on-chip antenna designed using standard CMOS technology, featuring a metasurface implementation on two-layer 500 μm-thick polyimide substrates. The two layers are separated by a 3 μm-thick aluminum ground plane, which is carved with concentrated dielectric rings beneath the radiation patches on the top layer. The structure demonstrates the characteristics of a metasurface, with an average

radiation gain and efficiency of 8.15 dBi and 65.71%, respectively, and a high bandwidth of 0.350–0.385 THz. The 6 x 6 x 1 mm^3 size makes it suitable for on-chip implementation.

In [14], several iterations of planar THz antennas were designed with different PBG-based substrates, operating at 0.63 THz. A homogeneous polyimide substrate antenna was used as a comparison. The Type-D antenna, supported by a circular unit cell PBG substrate, demonstrated superior gain ($> 9.4dB$), directivity ($> 10dB$), and impedance bandwidth ($> 29GHz$). The study examined the impact of varying the radii of the circular insertions on the antenna's gain and return loss. The results indicate that the THz antennas reported in this work show improvements in gain and bandwidth compared to other published THz antennas, making the antenna a viable option for current THz applications such as sensing, spectroscopy, medical diagnostics, and high-speed wireless hotspots.

In [7], the authors describe a prototype of a 2x3 antenna array, constructed on a 125 μm-thick polyimide dielectric substrate, operating between 0.19 and 0.20 THz. The array's dimensions are 20 x 13.5 x 0.125 mm^3. A 500 nm coating of graphene was applied to the antenna's metallization. The metamaterial-inspired design demonstrated an average improvement of 28 dB, 6.3 dBi, and 34% in isolation, radiation gain, and efficiency compared to the reference array. These findings suggest that the proposed method is viable for developing antenna arrays intended for use in integrated circuits operating below 1 GHz.

Graphene, a single layer of carbon atoms arranged in a hexagonal lattice, boasts exceptional electronic properties. Its conductivity can be dynamically adjusted by applying an electric field through an external gate voltage, which affects the material's chemical potential and, in turn, its conductivity. This external voltage shifts the Fermi level, allowing for precise control over the charge carrier density in graphene. This adjustability is a result of graphene's unique band structure, featuring a linear dispersion relation near the Fermi level. Consequently, graphene's electrical properties can be finely tuned, making it highly versatile for use in electronic devices, sensors, and other nanotechnology

applications. Harnessing this dynamic control of graphene's conductivity opens up new possibilities for developing advanced and high-performance electronic components.

The shift towards graphene-based microstrip patch antennas marks a significant step forward in antenna technology, overcoming the limitations of traditional metallic designs and enhancing performance in communication systems and wireless applications. As research and technological advancements continue, the exploration of the terahertz band for improved data transmission holds the potential to revolutionize communication systems and accelerate the evolution of IoT technologies. The unique characteristics of the THz spectrum, such as its ability to penetrate various materials and support high-bandwidth communication, make it a strong candidate for addressing the increasing demands of IoT networks.

As millimeter-wave technology advances towards commercial deployment, driven by the need for more bandwidth, the terahertz (THz) band is emerging as the next frontier in communication. In today's context, the need for improved channel capacity and high data rates is critical for wireless communication to meet new challenges. This proposal aims to utilize technical expertise in antenna design to develop and optimize novel metamaterial structures specifically for terahertz frequency applications. By integrating knowledge in antenna design, metamaterials science, and communication engineering, this project seeks to push the boundaries of terahertz technology, opening up new possibilities for information and communication technologies in this rapidly evolving field.

Table 2.1: Comparison of recent studies on THz metamaterial antennas.

Cite No.	Author	Publication	Description	Bandwidth (THz)
[15]	Vishwanath, Gaurav Varshney, Bikash Chandra Sahana	2024 Optical and Quantum Electronics	Design of tunable THz dielectric resonator antenna with cross-slot for circular polarization.	0.42
[16]	Ravinder Singh, Gaurav Varshney	2023 Optical and Quantum Electronics	Isolation enhancement technique in a dual-band THz MIMO antenna with single radiator.	0.36
[17]	Nishtha, Rajveer Singh Yaduvanshi, Gaurav Varshney	2023 Optical and Quantum Electronics	Isolation control for implementing the single dielectric resonator based tunable THz MIMO antenna and filter.	0.25
[18]	Mohd Farman Ali, Aarika Srivastava, Shreya Vijayvargiya, Gaurav Varshney	2023 Optical and Quantum Electronics	Compact tunable terahertz self-diplexing antenna with high isolation.	0.72

Cite No.	Author	Publication	Description	Bandwidth (THz)
[19]	A. Sivasangari, D. Deepa, P. Ajitha, R. M. Gomathi, R. Vignesh, Sathish Kumar Danasegaran, S. Poonguzhali	2023 Journal of Electronic Materials	Performance Analysis of Metamaterial Patch Antenna Characteristics for Advanced High-Speed Wireless System.	0.22
[20]	S. M. Shamim, Youssef Trabelsi, Nahid Arafn, N. K. Anushkannan, Umme Salma Dina, Md. Arafat Hossain, Nazrul Islam	2023 Optical and Quantum Electronics	Design and analysis of microstrip patch antenna with photonic band gap (PBG) structure for high-speed THz application.	0.27

2.3 Research Gap

Through the literature review and analysis, several research gaps have been identified that need to be addressed. These challenges range from the limited bandwidth availability to the complexities involved in selecting suitable materials for practical antenna implementation.

(i) Although current antennas offer certain benefits, their limited bandwidth hinders their application across the broad THz spectrum. To accommodate a wider array of uses within this frequency band, there is a clear need for compact, lightweight antennas with broad operational bandwidths.

(ii) A significant challenge in developing THz patch antennas lies in choosing the right materials and dimensions. The design process is often both time-consuming and

expensive, requiring careful consideration of various factors including performance, material costs, and practical properties. For example, while a substrate with a relative permittivity (ϵ_r) of 30 may produce promising simulation results, such materials are often impractical for real-world applications.

(iii) Current studies indicate that most THz antennas have dimensions larger than $100\mu m$. However, there is considerable potential to reduce antenna sizes even further. Smaller antennas could enhance the integration of THz communication technology into more compact devices and systems, thereby expanding the range of possible applications. Additionally, reducing antenna dimensions could facilitate the use of THz-enabled devices in confined spaces, such as in medical implants or wearable electronics, thus improving the scalability and accessibility of THz technology.

2.4 Objective

The primary goal of this proposal is to leverage expertise in antenna design to develop and optimize innovative metamaterial structures specifically for terahertz (THz) frequency applications. Additionally, the project aims to explore how these structures can be incorporated into high-speed communication systems. The specific objectives of the project are as follows:

(i) Conduct a comprehensive review and analysis of existing literature on the THz spectrum, metamaterials, and their application in antenna design.

(ii) Implement and refine antenna designs based on key research papers using the CST Studio Suite 2020 simulation software.

(iii) Perform simulations and assess deviations in the frequency spectrum to validate the proposed approach.

(iv) Carry out parametric studies and simulations using the electromagnetic (EM) simulator CST Studio Suite 2020 to achieve the desired results.

3

Proposed Methodology Design - 1

This section will outline the full methodology and implementation details of the project. It will discuss the antenna design and the materials chosen for the project, the methodology proposed, and the steps involved in executing the process.

3.1 Antenna design

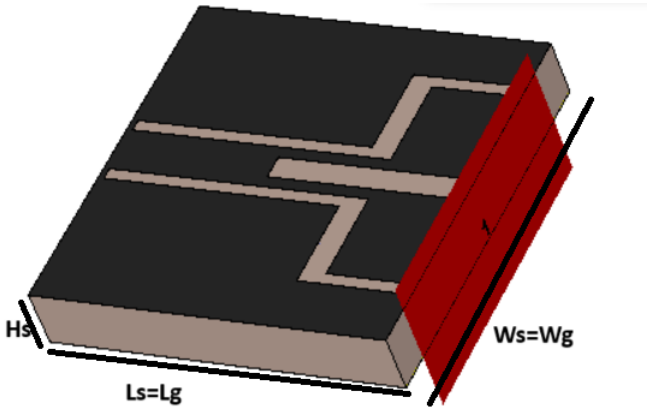

Figure 3.1: Antenna Dimensions 1

3.1.1 Antenna materials and dimensions

The schematic diagrams of the proposed THz patch antenna are illustrated in Fig. 3.1 and Fig. 3.2. The antenna design features a square patch with slits embedded within the patch. The antenna is composed of three key components: the ground plane, the substrate, and the radiating patch. The choice of materials and the precise calculation of dimensions are critical factors that significantly influence the antenna's performance. Graphene metamaterial is used for designing the radiating patch of the proposed antenna. Moreover, the substrate was designed using Polyimide $\epsilon_r = 3.5$ and the ground plane was designed using the Copper metal. Graphene, as a conductive material, boasts outstanding optical, chemical, mechanical, and electrical properties. It features low power consumption, exceptionally high carrier mobility, and a notably fast mean free path. The substrate material provides mechanical support for the antenna. The performance of the antenna components can be affected by the substrate material's relative permittivity (ϵ_r). An Graphene metamaterial-based 50 (Omega) microstrip line is used to excite the suggested antenna. The antenna design process takes multiple design iterations in order to achieve the desired result, however it is not always possible to conduct such process in

the real world. Therefore the antenna is designed, simulated and analysed on a virtual electromagnetic simulation software CST Studio Suite 2020. Table 3.1 gives the structural parameters of the proposed antenna.

Table 3.1: Antenna dimensions

Antenna Parameters	**Value**(μm)	**Antenna Parameters**	**Value**(μm)
Hs	10.04	Aw	2
Ls	60	Bl	32
Lg	60	Bw	4
Ws	60	Cl	18
Wg	60	Cw	2
Al	40	Dl	15

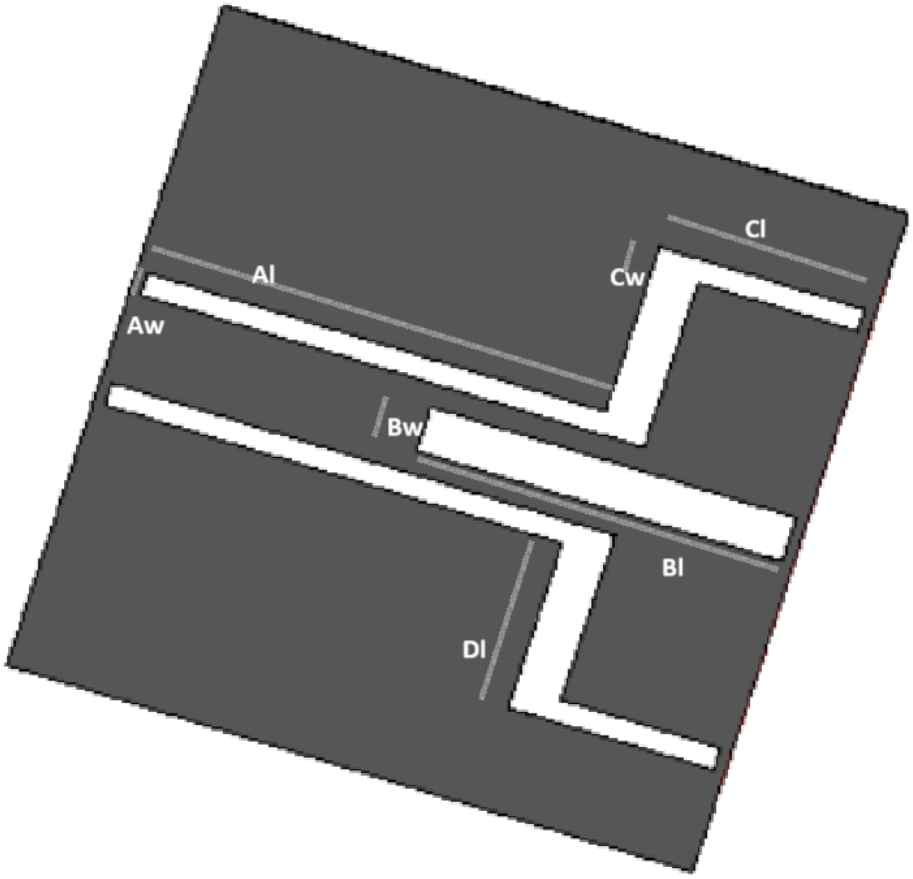

Figure 3.2: Antenna Dimensions 2

Before we begin with our antenna design process, we need to figure out the geometric

dimensions of our antenna. The dimension are calculated using various mathematical equations. Various formulas used are given in equation (3.1)-(3.4)

$$\epsilon_{reff} = \frac{\epsilon_r + 1}{2} + \frac{\epsilon_r - 1}{2} \left(\frac{1}{\sqrt{1 + \frac{2h}{W}}} \right) \tag{3.1}$$

Here ϵ_{reff} is effective dielectric constant of the substrate, h is height of the substrate material, ϵ_r is dielectric constant of a substrate and W is width of slot

$$W = \frac{1}{2 \times f_r \sqrt{\mu} \times \epsilon 0} \times \sqrt{\frac{2}{\epsilon r + 1}} \tag{3.2}$$

Here W = slot width, μ is permeability of free space, f_r is resonant frequency, ϵ_r is dielectric constant, ϵ_0 is permittivity of free space.

$$\frac{\Delta L}{h} = 0.412 \frac{(\epsilon_{reff} + 0.3)\left(\frac{W}{h} + 0.264\right)}{(\epsilon_{reff} + 0.258)\left(\frac{W}{h} + 0.8\right)} \tag{3.3}$$

$$L = \frac{c}{2 f_r \sqrt{\epsilon_{reff}}} - 2\Delta L \tag{3.4}$$

Here c speed of light.

3.1.2 Antenna Design Process

The dielectric constant $\epsilon_r = 3.5$, the thickness (Hs) of 10 μm, and the dielectric loss tangent (tan δ) of 0.0027 characterise the lossy polyimide substrate on which the proposed antenna structure is developed. Fig. 3.1 illustrates the simulated antenna's optimised design. The metamaterial structure consists of a square-shaped patch on the top surface of the substrate, while the bottom surface, or ground plane, is covered by a square metallic structure made of copper. The feedline has a width of 5μm. Graphene with a thickness of 0.035 μm is used to make the feedline, square-shaped patch. Several stages were taken in the patch design process in order to arrive at the final design that is seen in Fig. 3.3. First, as indicated in Step 1 of Fig. 3.3, a square patch measuring 60x60μm^2 is designed on the substrate material's top surface. Additionally, a metallic resonator rectangle with

dimensions of 4 x 32 μm^2 is loaded into the core square patch structure. Subsequently, two metallic resonator rectangles with dimensions of 15 x 4 μm^2 are loaded into the core square patch structure to create the structure seen in Step 2 of Figure 3.3. Next, as seen in Step 3 of Fig. 3.3, two rectangular shaped patch fed into the central square resonator. To create the final antenna design illustrated in phase 4 of Fig. 3.3, this patch is loaded with another two rectangular shaped structures in the last step 4. With the use of the computer simulation technology microwave studio suite (CST MWS) version 2020 software, the suggested antenna shape is created and examined. A waveguide port that is positioned at the feedline's bottom excites the antenna during the simulation. To achieve improved simulation accuracy, a tetrahedral mesh with adaptive mesh refinement is used for the subdivision of the structure into a large number of tetrahedrons during simulation.

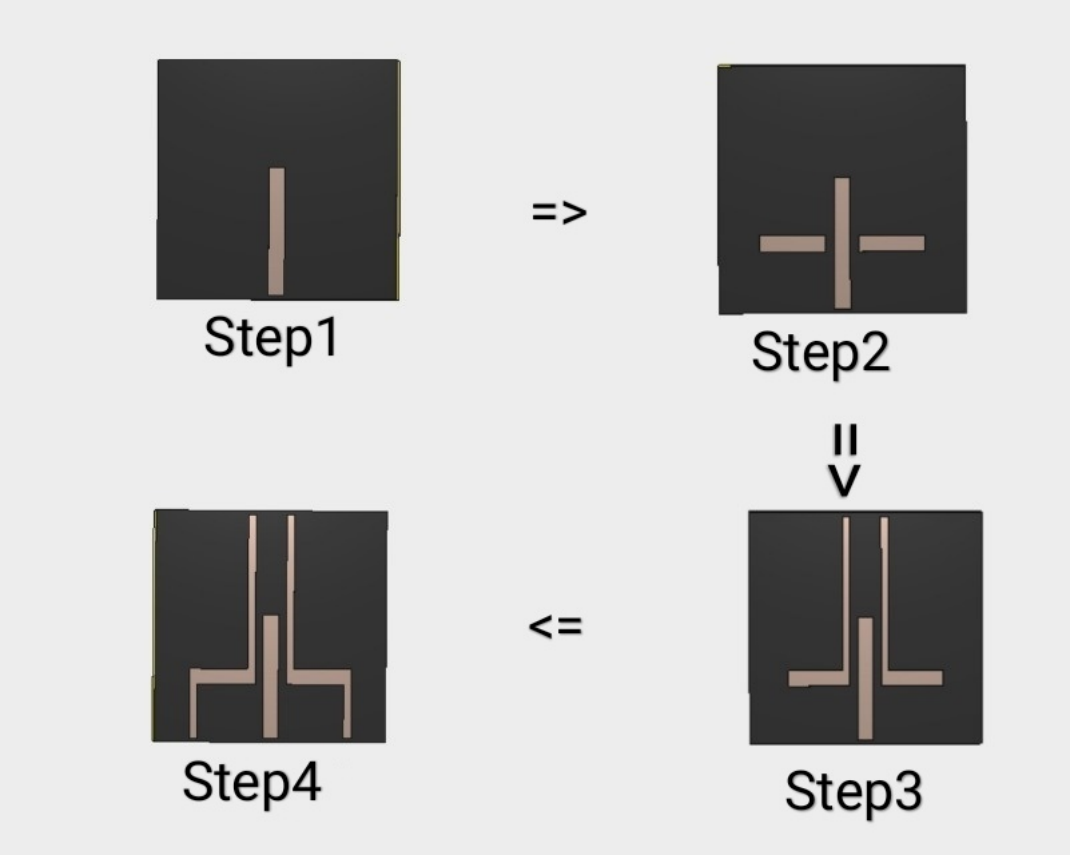

Figure 3.3: Step-wise Antenna Design Evolution

3.2 Results and Discussions

3.2.1 Design Step Evolution

As described in the section 3.1.2 of this work, during the design process, various iterations of the Terahertz antenna were designed simulated and the their performance was analysed in order to reach the final design. The antenna S11 performance at various steps of the design evolution process are shown below in the Fig.3.4. Table 3.2 describes effect of the various design steps and their operating frequency bands and their associated bandwidths in detail.

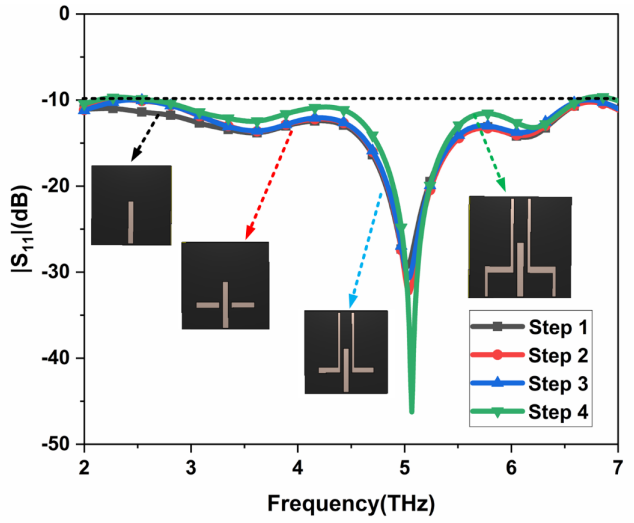

Figure 3.4: Step Evolution Return Loss Graph

Table 3.2: Step-wise S11 Bandwidth Table

Step	Frequency Range(THz)	Bandwidth(THz)	Total Bandwidth(THz)
Step 1	3.26 - 3.77 5.69 - 7.40	1.24 2.42	3.66 THz
Step 2	3.5 - 5.1 5.78 - 7.14	2.1 2.01	4.11 THz
Step 3	2.4 - 5.08 6.03 - 7.54	1.68 2.40	4.08 THz
Step 4	2.51 - 5.05 5.99 - 7.43	2.54 1.44	3.98 THz

3.2.2 Return Loss/S11

The proposed antenna is designed for wide-band THz frequency applications. For optimal performance, it's well-known that an antenna should have a reflection coefficient of less than -10 dB. This antenna resonates at 5.06 THz, with reflection coefficients of -47 dB, respectively, as shown in Fig. 3.5.

Additionally, the antenna exhibits robust performance across a range of frequency bands, ensuring its effective operation in specialized applications. This adaptability significantly enhances the antenna's versatility, making it well-suited for a wide variety of uses, including spectroscopy, biosensing, and advanced communication systems.

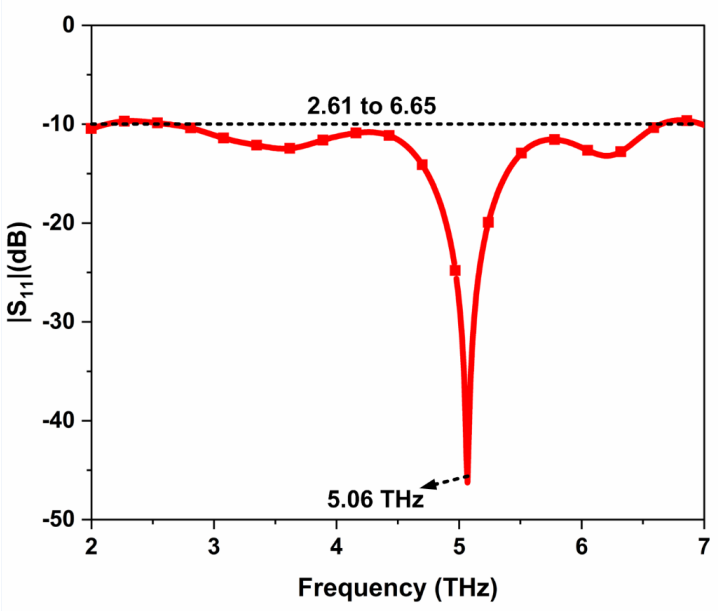

Figure 3.5: S11 Return Loss

3.2.3 VSWR

The graph in Fig. 3.6 illustrates the Voltage Standing Wave Ratio (VSWR) curve for the proposed antenna. The favorable reflection coefficient and VSWR values indicate proper impedance matching across the operational bands. To achieve optimal matching between the source and antenna impedance, the VSWR should remain below 2. Throughout the operational frequency ranges of 2.61-6.65 THz, the VSWR value is less than 2.

The VSWR values obtained verify the lowest possible mismatch losses.

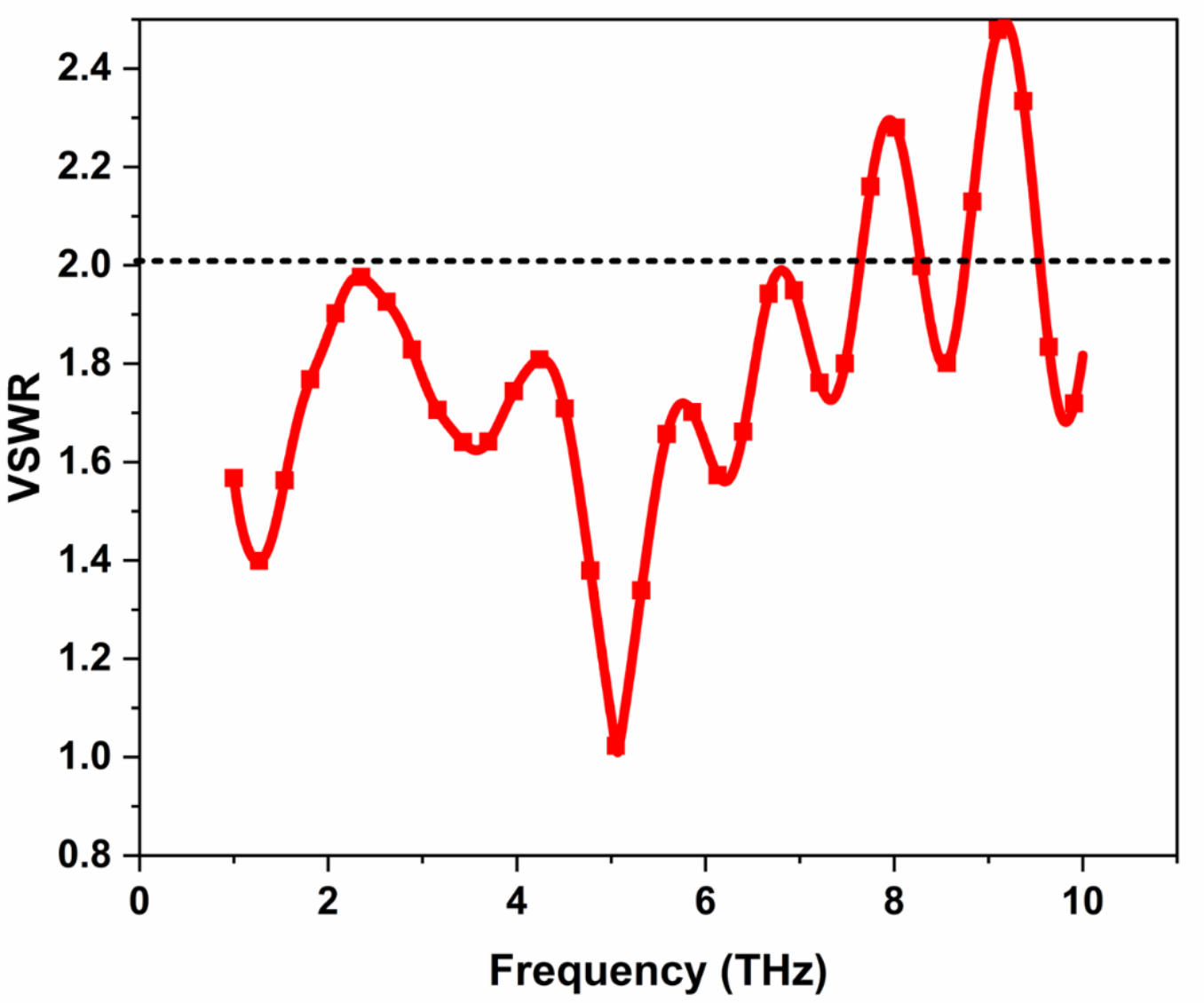

Figure 3.6: VSWR

3.2.4 Radiation Patterns

In Figure 3.7, the co-polar and cross-polar radiation patterns for both the electric field (E-field) and magnetic field (H-field) are illustrated across different resonant frequencies. These patterns illustrate how electromagnetic waves propagate in different directions relative to the antenna or radiating element. Copolar radiation patterns demonstrate the distribution of electromagnetic energy along the same polarization axis as the transmitting

antenna, while crosspolar patterns showcase energy distribution perpendicular to this axis. By examining these patterns at different resonant frequencies, engineers and researchers can gain insights into the behavior and performance of the antenna system across the electromagnetic spectrum. Grasping these patterns is essential for fine-tuning antenna designs tailored to specific applications, such as telecommunications, radar systems, or wireless networking.

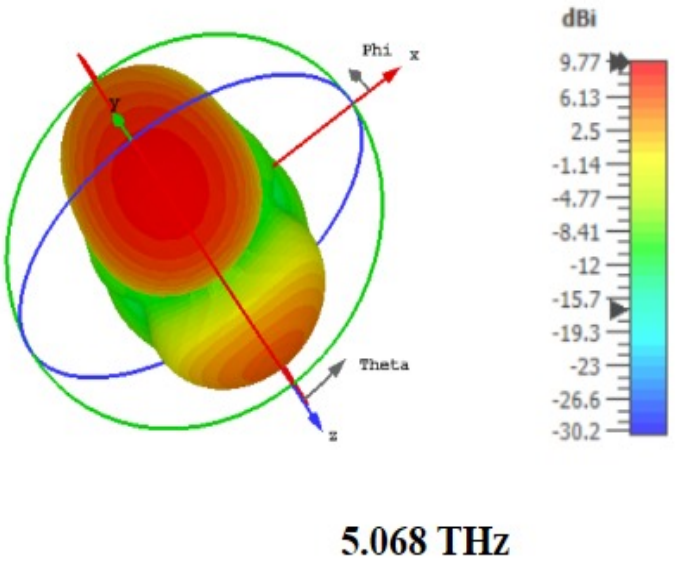

Figure 3.7: Radiation Patterns at 5.068 THz

These patterns illustrate how electromagnetic energy is distributed relative to the antenna's polarization axis. This information is valuable for optimizing antenna designs, ensuring effective performance across various applications and frequencies within the electromagnetic spectrum.

3.2.5 Surface Current

The surface current at various resonant frequencies are shown below in the Fig.3.8.

3.2.6 Impact of Various Materials

The antenna S11 performance at various steps of the design evolution process is observed during the simulation. The following table describes the impact of various antenna

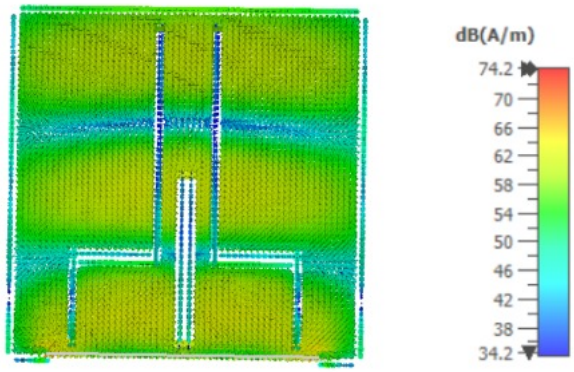

Figure 3.8: Surface Current

materials and their effects on the operating frequency bandwidths in detail.

Table 3.3: Substrate Materials and Associated Values

Substrate	**Rogers 5880**	**Polyimide**	**SiO_2**	**Quartz**
Graphene	2.84 - 3.92	2.34 - 5.24	2.47 - 4.61	2.74 - 4.71
		5.87 - 7.51	5.65 - 6.99	5.61 - 7.14
Copper	5.74 - 8.34	4.74 - 6.74	4.24 - 6.48	4.24 - 6.66
			8.04 - 9.32	8.27 - 9.66
Aluminium	5.62 - 6.33	4.43 - 6.87	4.18 - 6.49	4.26 - 6.60
			8.06 - 9.4	8.17 - 9.63
Gold	5.60 - 8.34	4.43 - 6.80	4.14 - 6.43	4.22 - 6.64
			8.09 - 9.49	8.15 - 9.65

4

Proposed Methodology Design - 2

The complete methodology is discussed in this section, along with the implementation details. The discussion will revolve around the antenna design and the materials used for the implementation of this project, the methodology proposed in this work, and the working process of the same.

4.1 Antenna design

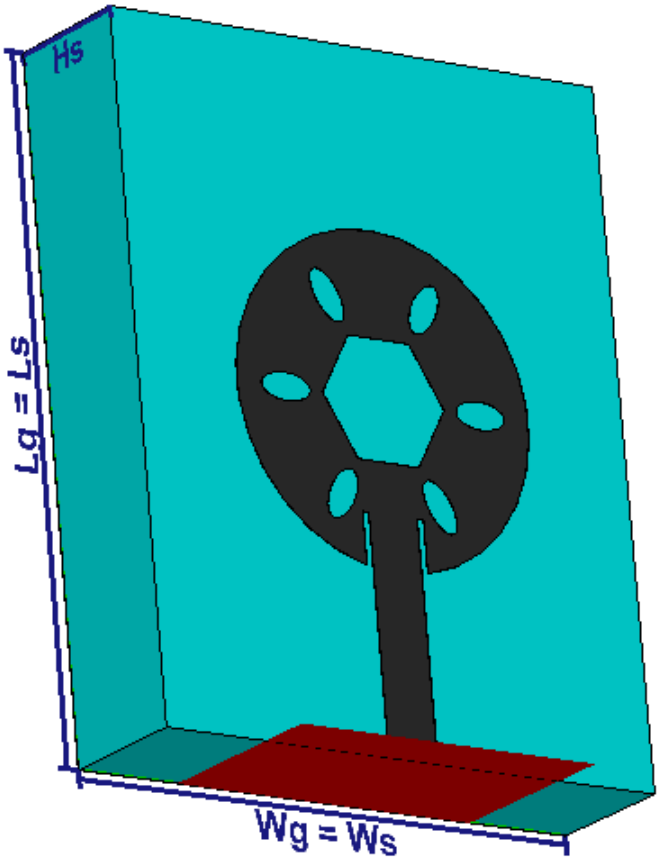

Figure 4.1: Antenna Dimensions 1

4.1.1 Antenna materials and dimensions

The schematic diagrams for the proposed THz patch antenna are illustrated below in Fig 4.1 and Fig 4.2. The proposed antenna features a circular patch with a hexagonal ring at center and six ellipse placed at each of the six corners. The design comprises three main components: the ground plane, the substrate, and the radiating patch. The selection of materials and precise calculation of dimensions are critical to the antenna's performance. Graphene is used for designing the radiating patch due to its exceptional optical, chemical, mechanical, and electrical properties. Specifically, graphene exhibits

low power consumption, high carrier mobility, and a rapid mean free path. The substrate is made of Silicon Dioxide ($\epsilon_r = 3.9$), while the ground plane is constructed using copper. The substrate material also provides mechanical support to the antenna, and its relative permittivity (ϵ_r) can significantly influence the antenna's performance. A graphene-based 50 Ω microstrip line is used to excite the proposed antenna. The design process involves multiple iterations to achieve the desired performance, which can be challenging to conduct in the real world. Therefore, the antenna is designed, simulated, and analyzed using CST Studio Suite 2020, a virtual electromagnetic simulation software. Table 4.1 gives the structural parameters of the proposed antenna.

Table 4.1: Antenna dimensions

Antenna Parameters	**Value**(μm)	**Antenna Parameters**	**Value**(μm)
Ws	40	Ls	50
Hs	10	Wg	40
Lg	50	d1	10
Lf	17	Wf	4
d2	4	d3	2
r	12	o	4

Before we begin with our antenna design process, we need to figure out the geometric dimensions of our antenna. The dimension are calculated using various mathematical equations. Various formulas used are given in equation (4.1)-(4.4)

$$\epsilon_{reff} = \frac{\epsilon_r + 1}{2} + \frac{\epsilon_r - 1}{2} \left(\frac{1}{\sqrt{1 + \frac{2h}{W}}} \right) \tag{4.1}$$

Here ϵ_{reff} is effective dielectric constant of the substrate, h is height of the substrate material, ϵ_r is dielectric constant of a substrate and W is width of slot

$$W = \frac{1}{2 \times f_r \sqrt{\mu} \times \epsilon 0} \times \sqrt{\frac{2}{\epsilon r + 1}} \tag{4.2}$$

Here W = slot width, μ is permeability of free space, f_r is resonant frequency, ϵ_r is dielectric constant, ϵ_0 is permittivity of free space.

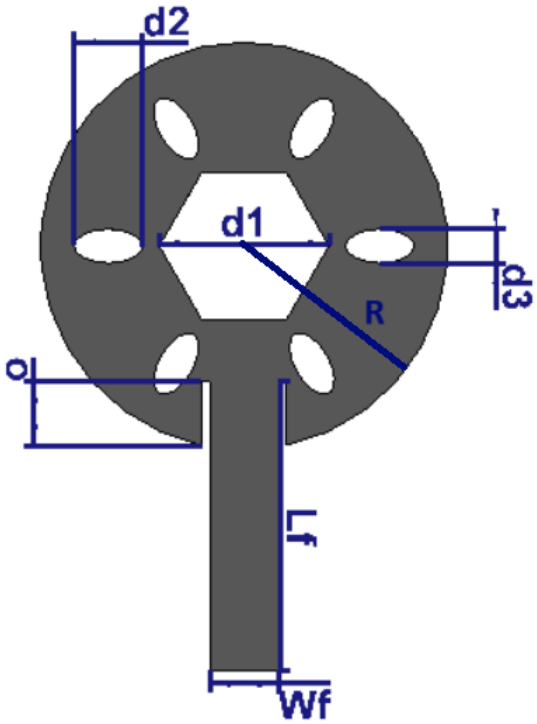

Figure 4.2: Antenna Dimensions 2

$$\frac{\Delta L}{h} = 0.412 \frac{(\epsilon_{reff} + 0.3)\left(\frac{W}{h} + 0.264\right)}{(\epsilon_{reff} + 0.258)\left(\frac{W}{h} + 0.8\right)} \tag{4.3}$$

$$L = \frac{c}{2f_r\sqrt{\epsilon_{reff}}} - 2\Delta L \tag{4.4}$$

Here c speed of light.

4.1.2 Antenna Design Process

The proposed antenna structure is developed on a lossy silicon dioxide substrate characterized by a dielectric constant $\epsilon_r = 3.9$, a thickness (H_s) of 10 μm, and a dielectric loss tangent (tan δ) of 0.0027. Fig. 4.1 presents the optimized design of the simulated antenna. The structure consists of a circular patch with a hexagon and surrounding ellipses on the corners of the hexagon. The bottom surface of the dielectric material, known as the ground plane, is covered by a square metallic structure made of copper. The feedline

has a width of 4 μm. Graphene with a thickness of 0.035 μm is used for the feedline, circular patch, and hexagonal ring.

Several steps were taken in the patch design process to arrive at the final design shown in Fig. 4.3. Initially, as shown in Step 1 of Fig. 4.3, a circular patch with a radius of 12 μm is created on the top surface of the substrate material. Next, a hexagonal metallic resonator ring with a radius of 5 μm is integrated into the central circular patch structure, as depicted in Step 2 of Fig. 4.3. Following this, as illustrated in Step 3 of Fig. 4.3, six ellipses with a center radius of major axis d_2 and minor axis d_3 are incorporated into the central circular resonator. To form the final antenna design, shown in Phase 4 of Fig. 4.3, these ellipses are added to the hexagonal patch after it has been shaped into a hexagon in the final Step 4. The proposed antenna design is created and analyzed using the Computer Simulation Technology Studio Suite (CST MWS) version 2020 software. During the simulation, the antenna is excited by a waveguide port located at the bottom of the feedline. For improved simulation accuracy, a tetrahedral mesh with adaptive mesh refinement is employed to divide the structure into a large number of tetrahedrons.

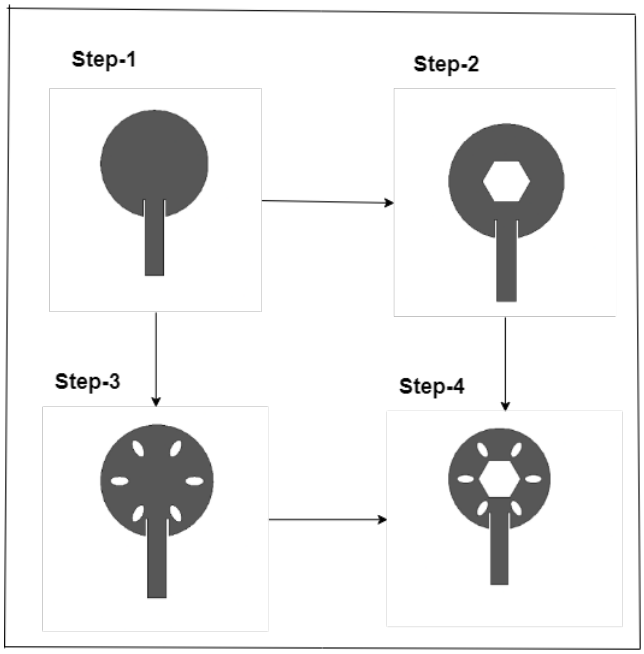

Figure 4.3: Step-wise Antenna Design Evolution

4.2 Results and Discussions

4.2.1 Design Step Evolution

As detailed in Section 4.1.2, the design process involved multiple iterations of the Terahertz antenna, with each version being designed, simulated, and evaluated to achieve the final design. Fig. 4.4 displays the S11 performance of the antenna at various stages of the design evolution. Table 4.2 provides a detailed description of the impact of different design steps on the operating frequency bands and their associated bandwidths.

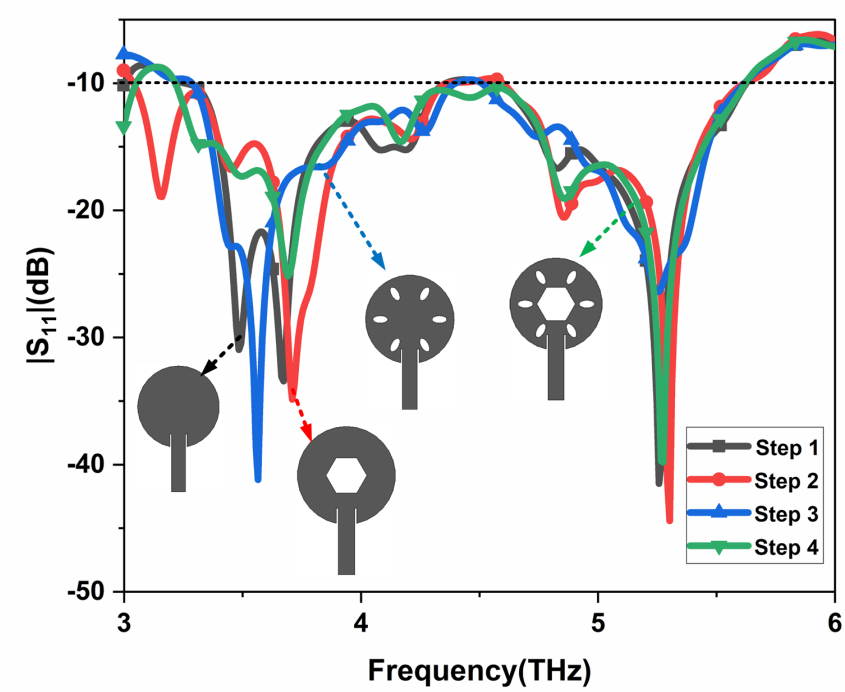

Figure 4.4: Step Evolution Return Loss Graph

Table 4.2: Step-wise S11 Bandwidth Table

Step	Frequency Range (THz)	Bandwidth (THz)	Total Bandwidth(THz)
Step 1	3.03 - 4.36 4.6 - 5.61	1.33 1.01	2.34
Step 2	3.04 - 4.36 4.6 - 5.62	1.32 1.02	2.34
Step 3	3.3 - 4.4 4.5 - 5.61	1.1 1.11	2.21
Step 4	3.21 - 5.62	2.41	2.41

4.2.2 Return Loss/S11

The proposed antenna is designed for broad-band applications within the THz frequency range. Achieving optimal impedance matching, usually indicated by a reflection coefficient lower than -10 dB, is essential for the antenna's performance. The design effectively resonates at two key frequencies: 3.69 THz and 5.27 THz, with impressive reflection coefficients of -25.2 dB and -39.71 dB, respectively, as depicted in Figure 4.5.

This antenna spans a wide bandwidth of 2.41 THz, covering frequencies from 3.21 THz to 5.62 THz. This extensive bandwidth enables the antenna to perform well in both wideband and narrowband applications, enhancing its versatility. Such broad frequency coverage makes it suitable for a range of uses, including advanced spectroscopy, sensitive biosensing, and high-performance communication systems. Its reliable operation across a wide frequency range highlights its adaptability and potential for various technological applications.

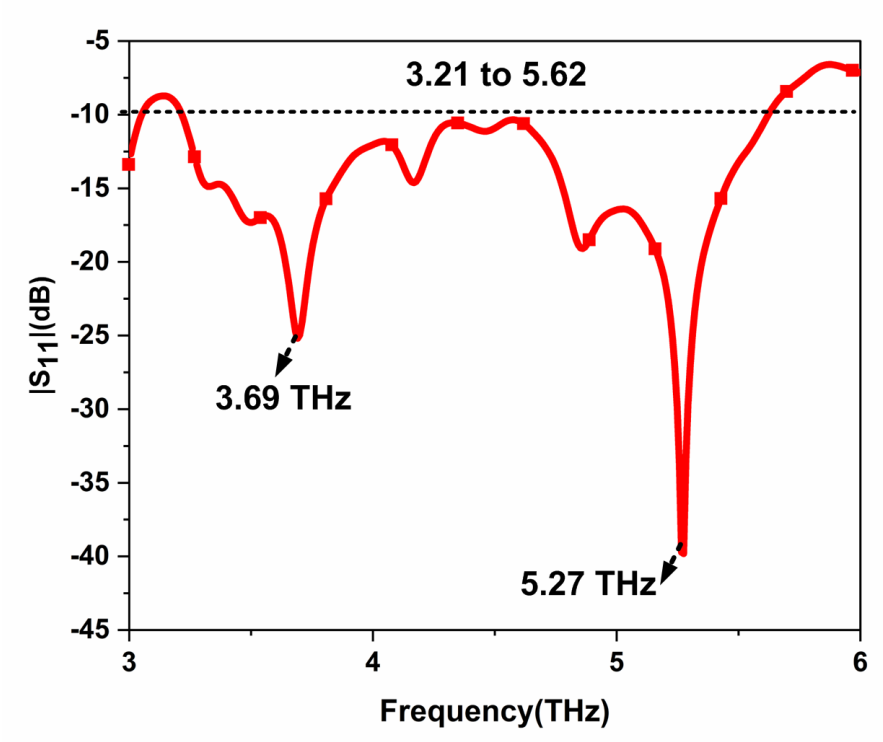

Figure 4.5: S11 Return Loss

4.2.3 VSWR

Fig. 4.6 shows the Voltage Standing Wave Ratio (VSWR) curve for the proposed antenna. The reflection coefficient and VSWR values indicate effective impedance matching across the antenna's operating frequencies. For optimal performance, the VSWR should be below 2, which means the impedance of the source and the antenna are well-aligned. Within the frequency range of 3.216 to 5.622 THz, the VSWR values are between 1.88 and 1.97. These values suggest minimal impedance mismatch and confirm the antenna's ability to reduce losses due to impedance mismatches, ensuring efficient performance throughout its specified frequency range.

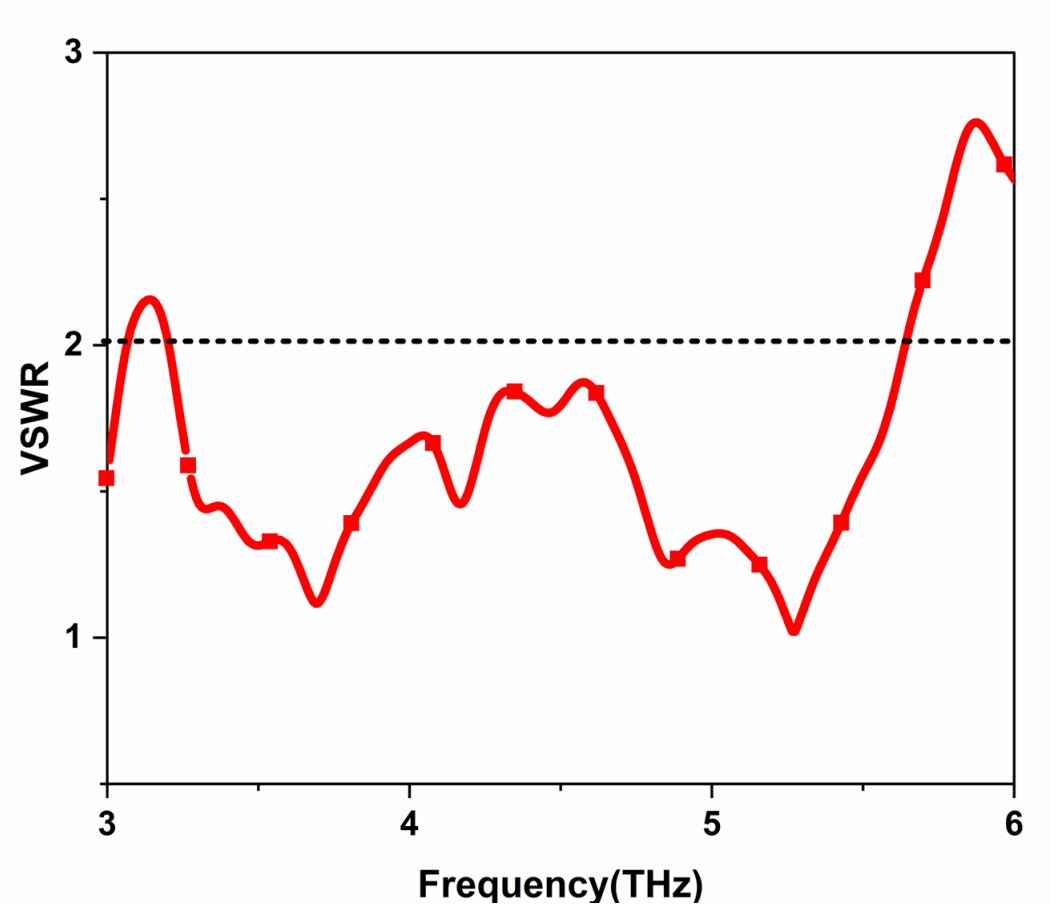

Figure 4.6: VSWR

4.2.4 Radiation Patterns

Fig. 4.7 displays the copolar and crosspolar radiation patterns for both the electric field (E-field) and magnetic field (H-field) at various resonant frequencies. These patterns illustrate how electromagnetic waves propagate in relation to the antenna or radiating element. Copolar radiation patterns show the distribution of energy aligned with the antenna's polarization axis, while crosspolar patterns show the distribution perpendicular to this axis. By examining these patterns across different resonant frequencies, engineers and researchers can gain a clearer understanding of the antenna system's performance and behavior across the electromagnetic spectrum. This insight is crucial for optimizing antenna designs for applications such as telecommunications, radar systems, and wireless networking.

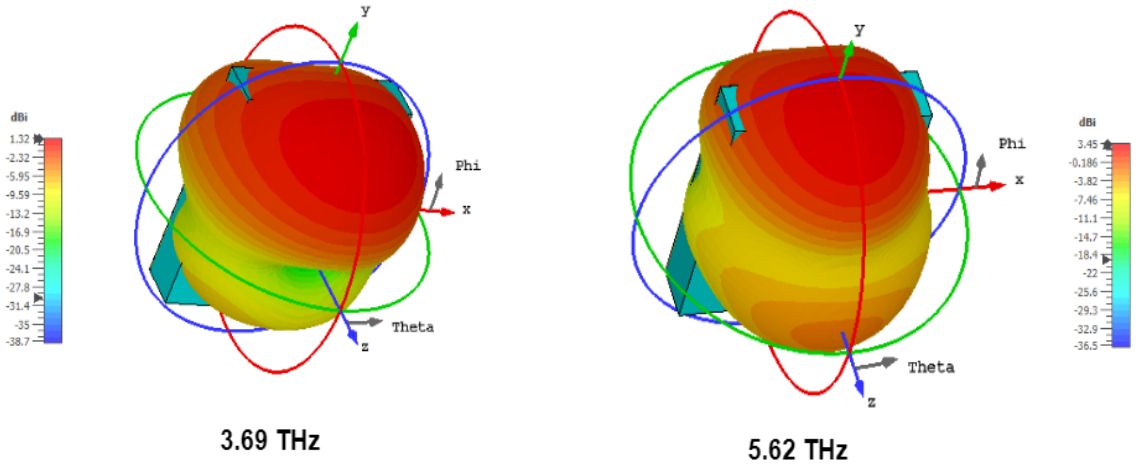

Figure 4.7: Radiation Patterns

These patterns demonstrate how electromagnetic energy is distributed in relation to the antenna's polarization axis. This data is crucial for refining antenna designs, ensuring optimal performance across different applications and frequencies within the electromagnetic spectrum.

4.2.5 Surface Current

Fig. 4.8 below displays the surface current at various resonant frequencies.

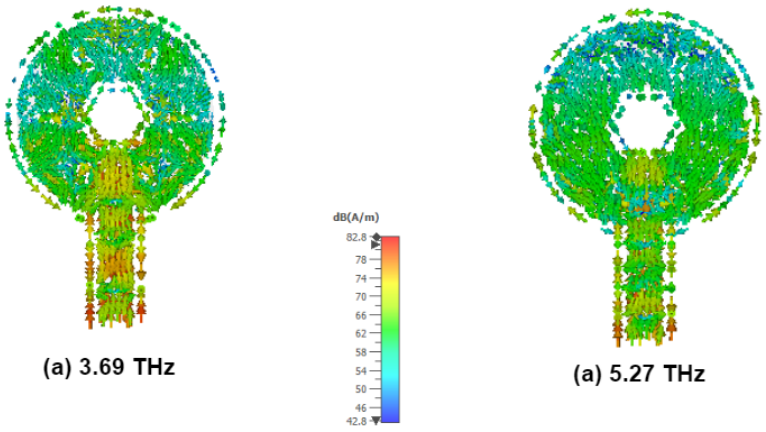

Figure 4.8: Surface Current

4.2.6 Impact of Various Materials

The antenna S11 performance at various steps of the design evolution process in the Table 4.3 that describes the impact of various antenna materials and their effects on the operating frequency bandwidths in detail.

Table 4.3: Substrate Materials and Associated Values

Substrate/ Patch	Rogers 5880	Polyimide	SiO_2	Quartz
Graphene	3.25 - 4.36 4.7 - 5.2	3.41 - 5.21	3.21 - 5.62	3.19 - 4.1 4.3 - 5.32
Copper	4.57 - 6.03	4.58 - 5.02 5.3 - 6.3	5.9 - 7.1	4.89 - 5.77 6.2 - 6.9
Aluminium	4.4 - 5.9	4.67 - 5.13 6.11 - 6.9	4.89 - 6.0 6.3 - 6.9	4.26 - 6.60
Gold	3.9 - 4.7 5.0 - 5.7	3.77 - 5.23 5.30 - 5.91	4.47 - 5.15 6.3 - 6.9	4.58 - 6

5

Proposed Methodology Design - 3

The complete methodology is discussed in this section, along with the implementation details. The discussion will revolve around the antenna design and the materials used for the implementation of this project, the methodology proposed in this work, and the working process of the same.

5.1 Antenna design

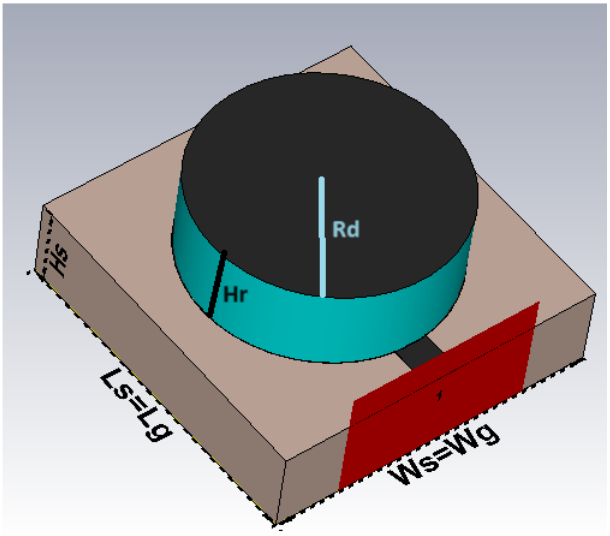

Figure 5.1: Antenna Dimensions 1

5.1.1 Antenna materials and dimensions

The schematic diagram of the proposed THz antenna, incorporating a Dielectric Resonator Antenna (DRA), is shown below in Fig 5.1 and Fig 5.2. The proposed antenna consists of a circular patch placed on top of the substrate, which is situated on a ground plane. The overall design includes three main components: the ground, the dielectric resonator, and the radiating patch.

For the radiating patch, **graphene metamaterial** is used, leveraging its properties. Graphene exhibits low power consumption, high carrier mobility, and a rapid mean free path, making it an ideal material for high-frequency applications.

The **DRA** is composed of **high-resistivity silicon (HRFZ-Si)**, selected for its low-loss characteristics and suitability for THz frequencies. The dielectric resonator is mechanically supported by a **Polyimide substrate** with a relative permittivity (ϵ_r) of 3.5. The ground plane is made from **copper metal**, providing the necessary conductive surface.

The substrate material's relative permittivity (ϵ_r) plays a crucial role in the antenna's

performance, particularly in maintaining high radiation efficiency and minimizing dielectric losses. A **graphene metamaterial-based 50 Ω microstrip line** is used to excite the proposed antenna, ensuring efficient power transfer and radiation.

The design of the antenna involves multiple iterations to achieve the desired results. However, due to the complexities of real-world prototyping, the antenna is designed, simulated, and analyzed using **CST Studio Suite 2020**. Table 5.1 provides the structural parameters of the proposed antenna, considering the inclusion of the DRA and the novel graphene patch design.

Table 5.1: Antenna dimensions

Antenna Parameters	**Value**(μm)	**Antenna Parameters**	**Value**(μm)
L	13	Ls	40
R	15	Lg	40
Lf	5	Ws	40
Wf	4	Wg	40
r	2	Hs	10
Rd	15	Hr	10

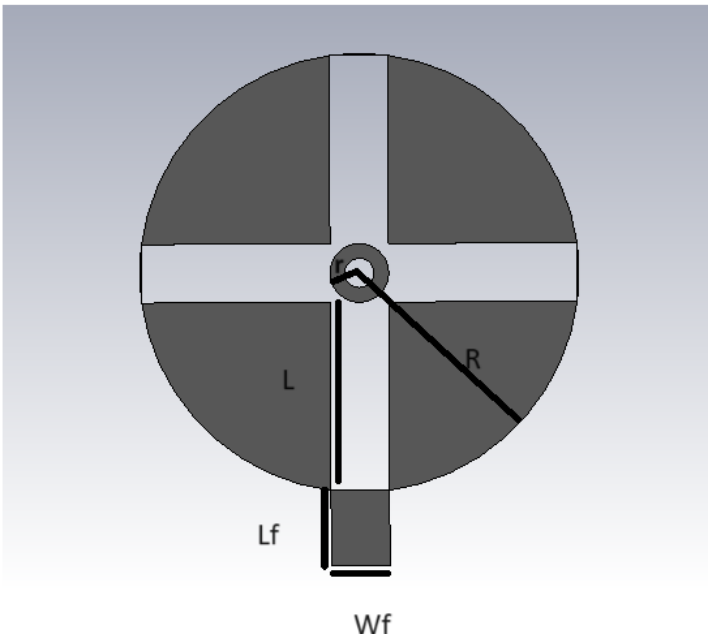

Figure 5.2: Antenna Dimensions 2

Before we begin with our antenna design process, we need to determine the geometric

dimensions of our antenna. These dimensions are calculated using various mathematical equations to ensure optimal performance at the desired resonant frequency. The relevant formulas are given in equations (5.1)-(5.4).

$$\epsilon_{reff} = \frac{\epsilon_r + 1}{2} + \frac{\epsilon_r - 1}{2} \left(\frac{1}{\sqrt{1 + \frac{2h}{W}}} \right) \tag{5.1}$$

Here, ϵ_{reff} is the effective dielectric constant of the substrate, h is the height of the substrate material, ϵ_r is the dielectric constant of the substrate, and W is the width of the slot.

$$W = \frac{1}{2 \times f_r \sqrt{\mu_0 \epsilon_0}} \times \sqrt{\frac{2}{\epsilon_r + 1}} \tag{5.2}$$

Here, W is the slot width, μ_0 is the permeability of free space ($4\pi \times 10^{-7}$ H/m), f_r is the resonant frequency, ϵ_r is the dielectric constant of the substrate, and ϵ_0 is the permittivity of free space (8.854×10^{-12} F/m).

$$\frac{\Delta L}{h} = 0.412 \frac{(\epsilon_{reff} + 0.3)\left(\frac{W}{h} + 0.264\right)}{(\epsilon_{reff} + 0.258)\left(\frac{W}{h} + 0.8\right)} \tag{5.3}$$

$$L = \frac{c}{2 f_r \sqrt{\epsilon_{reff}}} - 2\Delta L \tag{5.4}$$

Here, c is the speed of light in a vacuum (approximately 3×10^8 m/s), and ΔL is the length extension due to fringing fields.

These equations are critical in calculating the dimensions required for achieving the desired resonant frequency and bandwidth of the antenna. When designing an antenna, especially if incorporating a Dielectric Resonator Antenna (DRA) or using advanced materials like graphene, additional factors such as the DRA's height and the material's unique properties should be considered.

5.1.2 Antenna Design Process

The proposed antenna design features a lossy polyimide substrate with a dielectric constant (ϵ_r) of 3.5, a thickness (H_s) of 10 μm, and a dielectric loss tangent ($\tan\delta$) of 0.0027. The optimized antenna structure, as illustrated in Fig. 5.1, consists of a circular patch with slots forming a metamaterial pattern on the top surface of the substrate. The bottom surface is covered with a square metallic ground plane made of copper. The feedline, with a width of 2 μm, and the circular patch are both composed of graphene with a thickness of 0.035 μm. The design process leading to the final antenna configuration shown in Fig. 5.3 involved several stages. Initially, as depicted in Step 1 of Fig. 5.3, a circular patch with a radius of 15 μm was designed on the top surface of the substrate. In Step 2, a cross-slot forming a plus sign was added to the patch, along with a small concentric circle at its center. In Step 3, a Dielectric Resonator made from High Resistivity Silicon material was added on top of the patch. Finally, in Step 4, a thin layer of graphene, 0.34 nm thick, was applied to complete the antenna design.

The proposed antenna was designed and analyzed using CST Microwave Studio Suite (CST MWS) version 2020. During the simulation, a waveguide port located at the bottom of the feedline was used to excite the antenna. To achieve high simulation accuracy, the structure was divided into numerous tetrahedrons using a tetrahedral mesh with adaptive mesh refinement.

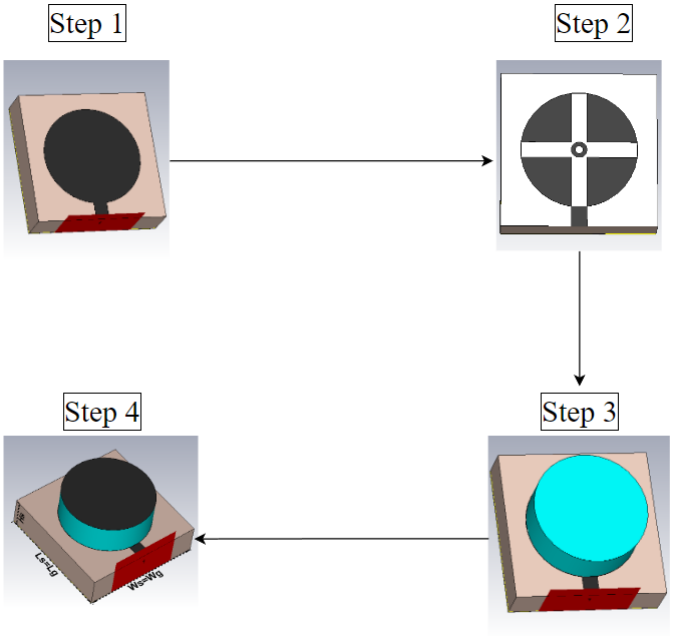

Figure 5.3: Step-wise Antenna Design Evolution

5.2 Results and Discussions

5.2.1 Design Step Evolution

As detailed in Section 5.1.2 of this work, the design process involved multiple iterations of the Terahertz antenna, where each version was meticulously simulated and its performance analyzed to refine and finalize the design. The progression of the antenna's S11 performance across these iterative design stages is illustrated in Figure 5.4. and table 5.2 provides a comprehensive overview of the impact of each design iteration, detailing the corresponding operating frequency bands and the associated bandwidths at each stage of the development process.

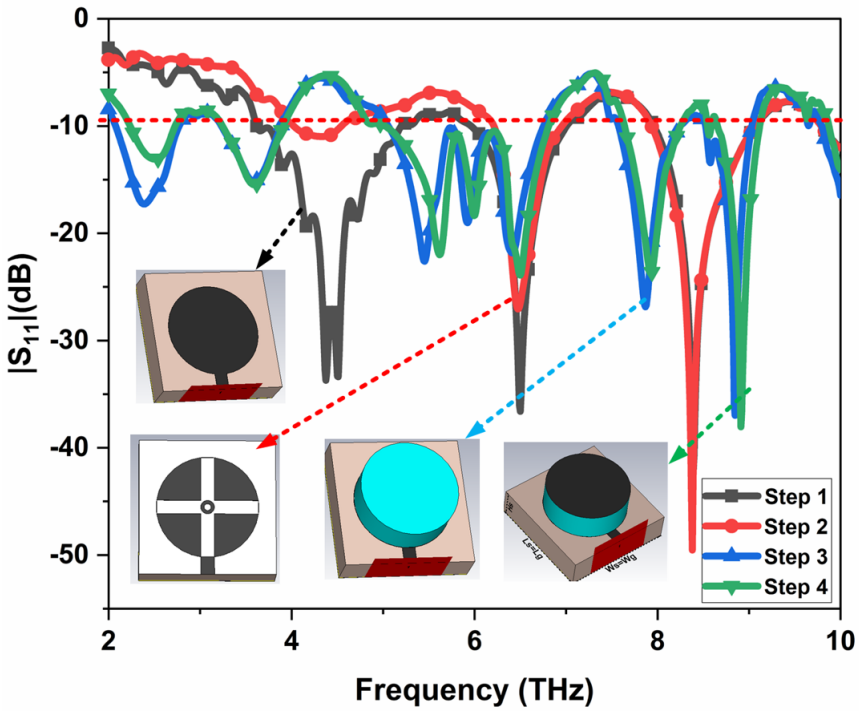

Figure 5.4: Step Evolution Return Loss Graph

Table 5.2: Step-wise S11 Bandwidth Table

Step	Frequency Range(THz)	Bandwidth(THz)	Total Bandwidth(THz)
Step 1	3.61- 5.19	1.58	
	5.94 - 7.01	1.07	
	7.95 - 9.07	1.12	3.77 THz
Step 2	6.21 - 6.96	0.75	
	7.94 - 9.07	1.13	1.88 THz
Step 3	5.05 - 6.75	1.70	
	7.57 - 8.24	0.67	2.89 THz
	8.51 - 9.03	0.52	
Step 4	5.02 - 6.82	1.8	
	7.64 - 8.24	0.6	2.86 THz
	8.65 - 9.11	0.46	

5.2.2 Return Loss/S11

The proposed antenna has been designed for application in multi-band THz frequency range applications. It is widely acknowledged that ideal impedance matching conditions for an antenna require a reflection coefficient of less than -10 dB. The proposed antenna resonates at 7.93 THz and 8.91 THz with reflection coefficients of -23.78 dB, -38.05,

respectively, as shown in Fig. 5.5.

The entire frequency range from 5.02 THz to 6.82 THz is covered by the antenna's wide operating bandwidth of 1.8 THz. Furthermore, we register two narrow bands with operating bandwidths of 0.6 THz and 0.46 THz, respectively, that span the frequency ranges of 7.64 THz to 8.24 THz and 8.65 THz to 9.11 THz.This ability to support both broad and narrowband specifications increases the antenna's adaptability and usefulness in a variety of contexts, including spectroscopy, biosensing, and communication systems.

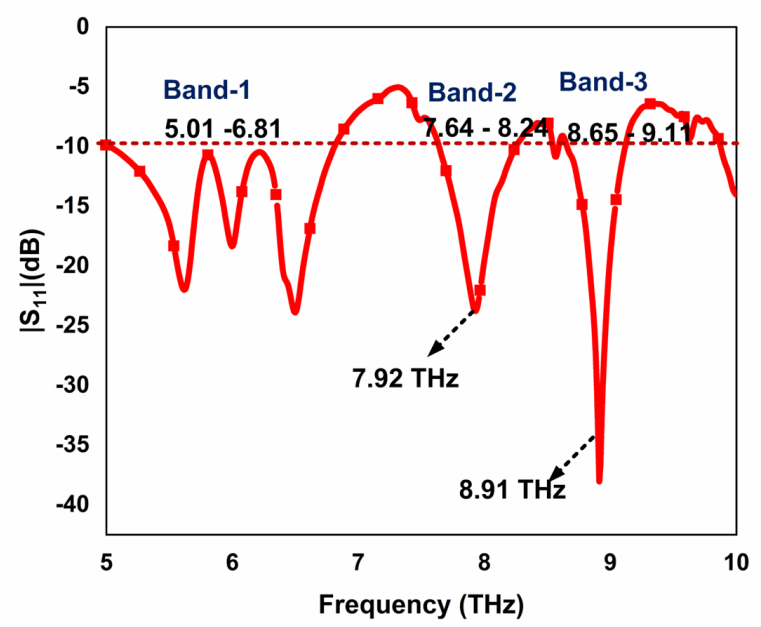

Figure 5.5: S11 Return Loss

5.2.3 VSWR

The graph in Fig.5.6 depicts the Voltage Standing Wave Ratio (VSWR) curve for the proposed antenna. The appropriate impedance matching of the suggested antennas throughout the operational bands is ensured by the desirable reflection coefficient and VSWR values. To ensure that the source impedance and antenna impedance are properly matched, the VSWR value should be less than 2. Throughout the operational frequency ranges of 5.01-6.82THz, 7.64-8.24THz, and 8.65-9.11THz, the VSWR value is between 1.88 and 1.97. The VSWR values obtained verify the lowest possible mismatch losses.

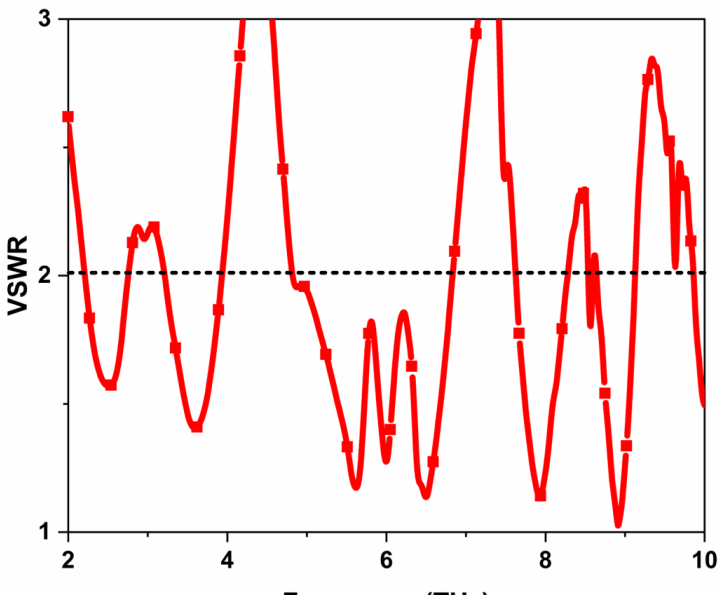

Figure 5.6: VSWR

5.2.4 Radiation Patterns

Figure 5.7 illustrates the copolar and crosspolar radiation patterns for both the electric field (E-field) and magnetic field (H-field) across different resonant frequencies. These patterns offer a detailed view of how electromagnetic waves propagate in various directions relative to the antenna or radiating element.

The copolar radiation patterns show the distribution of electromagnetic energy aligned with the antenna's polarization axis, which is important for assessing how effectively the antenna transmits energy in the desired direction. Conversely, the crosspolar patterns reveal the distribution of energy perpendicular to the main polarization axis, providing insights into unintended radiation and potential polarization mismatches.

Analyzing these radiation patterns at various resonant frequencies allows engineers and researchers to better understand the antenna's performance and behavior throughout the electromagnetic spectrum. This analysis is crucial for optimizing antenna designs for different applications, including telecommunications, radar systems, and wireless networks. These patterns not only reveal the directional distribution of electromagnetic energy but also provide essential information for fine-tuning antenna characteristics to achieve op-

timal performance in specific applications, thus enhancing overall system efficiency and effectiveness.

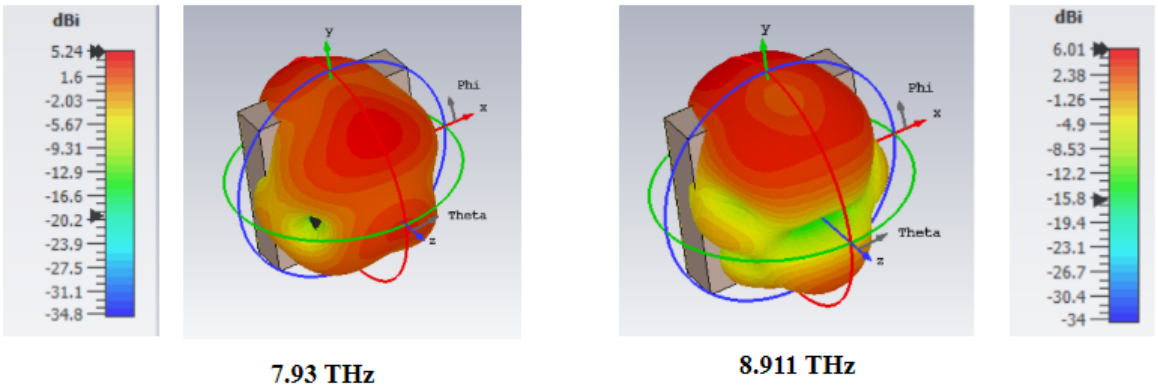

Figure 5.7: Radiation Patterns

These patterns show how electromagnetic energy is distributed in relation to the antenna's polarization axis, helping to refine antenna designs for various applications across the electromagnetic spectrum.

5.2.5 Surface Current

The surface current at various resonant frequencies are shown below in the Fig. 5.8.

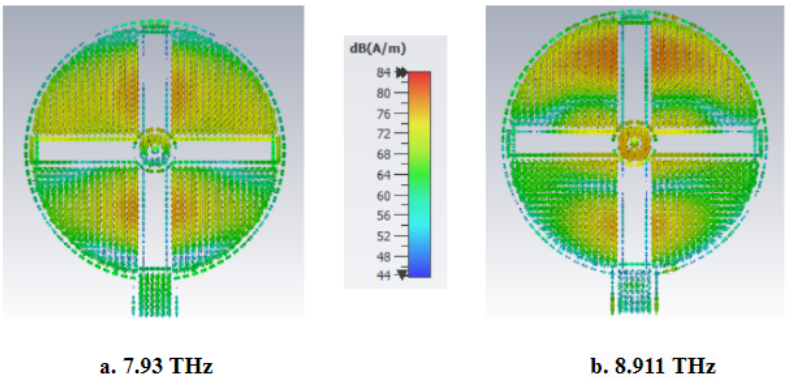

Figure 5.8: Surface Current

5.2.6 Impact of Various Materials

The antenna S11 performance at various steps of the design evolution process are shown below in Table 5.3 that describes the impact of various antenna materials and their effects on the operating frequency bandwidths in detail.

Figure 5.9: Materials Impact Graphs

Material	Rogers 5880	Polyimide	SiO_2	Quartz
Graphene	2.98 - 3.73	5.02 - 6.82	2.60 - 3.40	2.65 - 3.50
	4.94 - 5.97	7.64 - 8.24	5.65 - 6.20	5.75 - 6.28
	7.94 - 9.63	8.65 - 9.11	7.25 - 8.02	7.30 - 8.05
Copper	5.66 - 8.31	5.35 - 6.20	4.45 - 5.80	4.80 - 6.00
			7.90 - 8.50	8.15 - 8.95
Aluminium	5.62 - 6.33	5.25 - 6.10	4.43 - 5.50	4.70 - 5.60
			7.80 - 8.50	8.20 - 8.85
Gold	5.66 - 8.30	5.40 - 6.20	4.44 - 5.70	4.85 - 6.10
			7.85 - 8.60	8.10 - 8.90

Table 5.3: S11 Parameter Bandwidths Across Different Substrate-Material Combinations

6

Proposed Methodology Design - 4

This section offers a detailed overview of the methodology, including the specifics of the implementation. It will address the antenna design, the materials used for the project, the proposed approach, and the procedures involved in the operation.

6.1 Antenna design

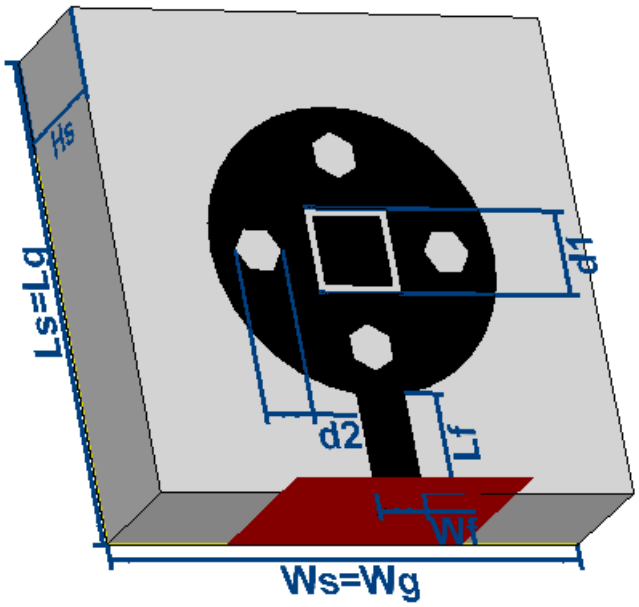

Figure 6.1: Antenna Dimensions 1

6.1.1 Antenna Materials and Dimensions

Figures 6.1 and 6.2 illustrate the schematic diagrams of the proposed THz patch antenna. The design features a circular patch, four hexagonal rings arranged both vertically and horizontally, and a central square. The antenna consists of three main components: the ground plane, the substrate, and the radiating patch. The materials selected and the accurate calculation of dimensions are crucial for the antenna's performance. The radiating patch is made from graphene metamaterial, the substrate is crafted from Polyimide with a relative permittivity of $\epsilon_r = 3.5$, and the ground plane is composed of copper. Graphene, as a conductive material, offers outstanding optical, chemical, mechanical, and electrical properties, characterized by low power consumption, high carrier mobility,

and a rapid mean free path. The substrate material provides mechanical support to the antenna, and its relative permittivity (ϵ_r) significantly impacts the performance of the antenna components. A 50 Ω microstrip line, also based on graphene metamaterial, is employed to excite the proposed antenna. The design process of the antenna involves multiple iterations to achieve the desired performance, which may not always be feasible in a physical setting. Consequently, the antenna is designed, simulated, and analyzed using CST Studio Suite 2020, a virtual electromagnetic simulation software. The structural parameters of the proposed antenna are detailed in Table 6.1.

Table 6.1: Antenna dimensions

Antenna Parameters	**Value**(μm)	**Antenna Parameters**	**Value**(μm)
Ws	40	Ls	40
d1	5	d2	2
Wg	40	Lg	40
Lf	9	Wf	4

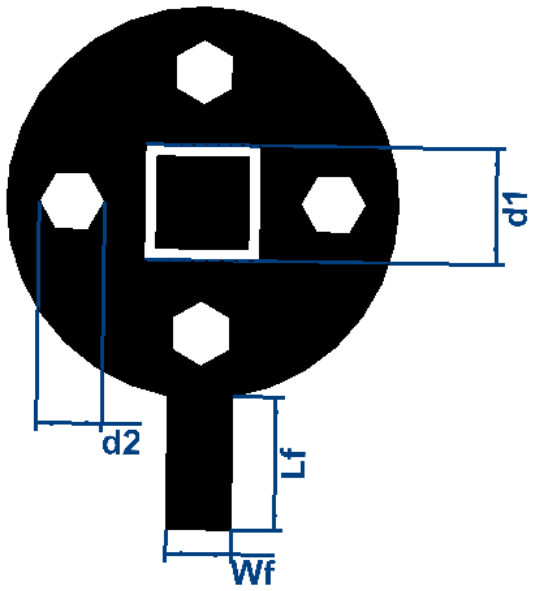

Figure 6.2: Antenna Dimensions 2

Before we begin with our antenna design process, we need to figure out the geometric

dimensions of our antenna. The dimension are calculated using various mathematical equations. Various formulas used are given in equation (3.1)-(3.4)

$$\epsilon_{reff} = \frac{\epsilon_r + 1}{2} + \frac{\epsilon_r - 1}{2} \left(\frac{1}{\sqrt{1 + \frac{2h}{W}}} \right) \tag{6.1}$$

Here ϵ_{reff} is effective dielectric constant of the substrate, h is height of the substrate material, ϵ_r is dielectric constant of a substrate and W is width of slot

$$W = \frac{1}{2 \times f_r \sqrt{\mu} \times \epsilon 0} \times \sqrt{\frac{2}{\epsilon r + 1}} \tag{6.2}$$

Here W = slot width, μ is permeability of free space, f_r is resonant frequency, ϵ_r is dielectric constant, ϵ_0 is permittivity of free space.

$$\frac{\Delta L}{h} = 0.412 \frac{(\epsilon_{reff} + 0.3)\left(\frac{W}{h} + 0.264\right)}{(\epsilon_{reff} + 0.258)\left(\frac{W}{h} + 0.8\right)} \tag{6.3}$$

$$L = \frac{c}{2 f_r \sqrt{\epsilon_{reff}}} - 2\Delta L \tag{6.4}$$

Here c speed of light.

6.1.2 Antenna Design Process

The proposed antenna structure is developed on a lossy polyimide substrate characterized by a dielectric constant $\epsilon_r = 3.5$, a thickness (Hs) of 10 μm, and a dielectric loss tangent (tan δ) of 0.0027. The optimized design of the simulated antenna is shown in Fig. 6.1. The metamaterial structure on the top surface of the substrate consists of a circular patch with slots and a square ring. The bottom surface of the dielectric material, referred to as the ground plane, is covered by a square metallic structure made of copper. The feedline, which has a width of 4 μm, is constructed from graphene with a thickness of 0.035 μm and is used for the feedline, circular patch, hexagonal, and square ring. The patch design process involved several steps to arrive at the final configuration depicted in Fig. 6.3. Initially, as shown in Step 1 of Fig. 6.3, a circular patch was designed on the

substrate material's top surface. Following this, in Step 2 of Fig. 6.3, a square metallic resonator ring with dimensions of 5X5 μm^2 was integrated into the core circular patch structure. Next, Step 3 of Fig. 6.3 introduced a circular patch with a centered square ring and two horizontal hexagonal rings into the central circular resonator. Finally, in Step 4 of Fig. 6.3, the design was completed by incorporating a circular patch, four hexagonal rings arranged in both vertical and horizontal directions, and a centered square. The proposed antenna design is created and analyzed using CST Microwave Studio (CST MWS) Suite 2020 software. During the simulation, the antenna is excited by a waveguide port positioned at the base of the feedline. To enhance simulation accuracy, the structure is subdivided into a large number of tetrahedrons using a tetrahedral mesh with adaptive mesh refinement.

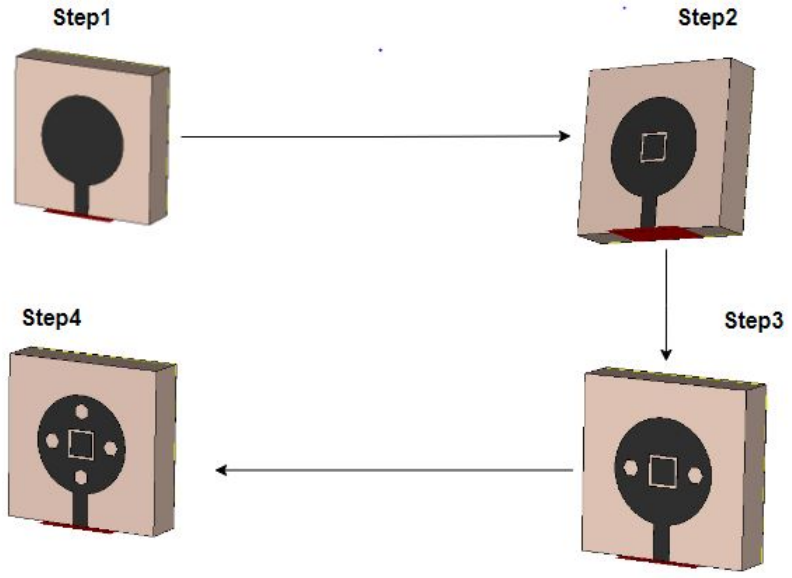

Figure 6.3: Step-wise Antenna Design Evolution

6.2 Results and Discussions

6.2.1 Design Step Evolution

As described in the section 6.1.2 of this work, during the design process, various iterations of the Terahertz antenna were designed simulated and the their performance

was analysed in order to reach the final design. The antenna S11 performance at various steps of the design evolution process are shown below in the Fig.6.4. Table 6.2 describes effect of the various design steps and their operating frequency bands and their associated bandwidths in detail.

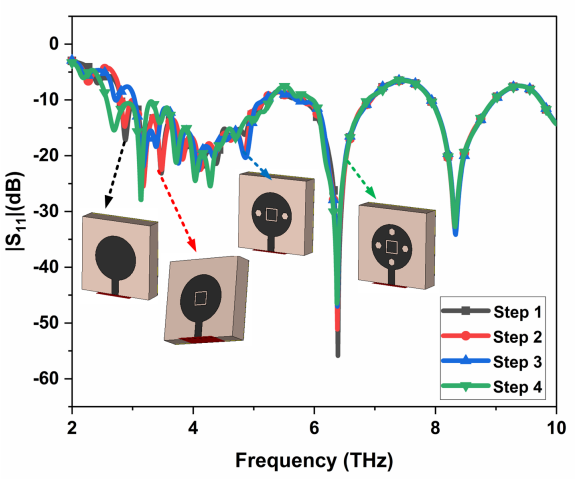

Figure 6.4: Step Evolution Return Loss Graph

Table 6.2: Step-wise S11 Bandwidth Table

Step	Frequency Range(THz)	Bandwidth(THz)	Total Bandwidth(THz)
Step 1	2.80- 5.22 5.82- 6.92 7.92 - 8.96	2.42 1.1 1.04	4.56THz
Step 2	2.80 - 5.17 5.80 - 6.93 7.92 - 8.96	2.37 1.13 1.04	4.54 THz
Step 3	3.01 - 5.17 5.72- 6.91 7.92 - 8.96	2.16 1.19 1.04	4.39 THz
Step 4	2.57 - 5.27 5.97 - 6.88 7.91 - 8.97	2.70 0.91 1.06	4.67 THz

6.2.2 Return Loss/S11

The proposed antenna is optimized for wide-band applications within the THz frequency range. For effective antenna performance, optimal impedance matching is typically achieved with a reflection coefficient below -10 dB. The antenna is tuned to resonate at 3.14 THz, 6.37 THz, and 8.32 THz, with reflection coefficients of -27.93 dB, -46.43 dB, and -32.76 dB, respectively, as shown in Fig. 6.5.

The antenna features a broad operating bandwidth of 2.70 THz, spanning from 2.57 THz to 5.27 THz. Additionally, it supports two narrower bands with bandwidths of 0.91 THz and 1.06 THz, covering the ranges from 5.99 THz to 6.88 THz and from 7.91 THz to 8.99 THz, respectively. This combination of wide and narrowband capabilities makes the antenna highly versatile and suitable for various applications, including spectroscopy, biosensing, and communication systems.

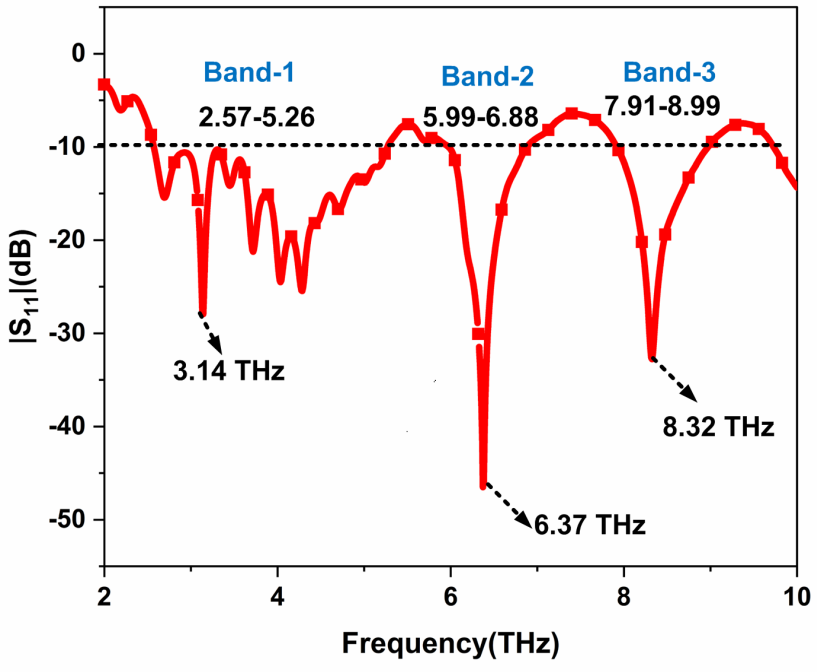

Figure 6.5: S11 Return Loss

6.2.3 VSWR

The graph in Fig. 6.6 illustrates the Voltage Standing Wave Ratio (VSWR) curve for the proposed antenna. The desirable reflection coefficient and VSWR values ensure proper impedance matching of the antenna across the operational frequency bands. For optimal matching between the source impedance and antenna impedance, the VSWR value should be less than 2. Within the operational frequency ranges of 2.57-5.26 THz, 5.99-6.88 THz, and 7.91-8.99 THz, the VSWR values remain between 1.65 and 1.85. These VSWR values confirm minimal mismatch losses..

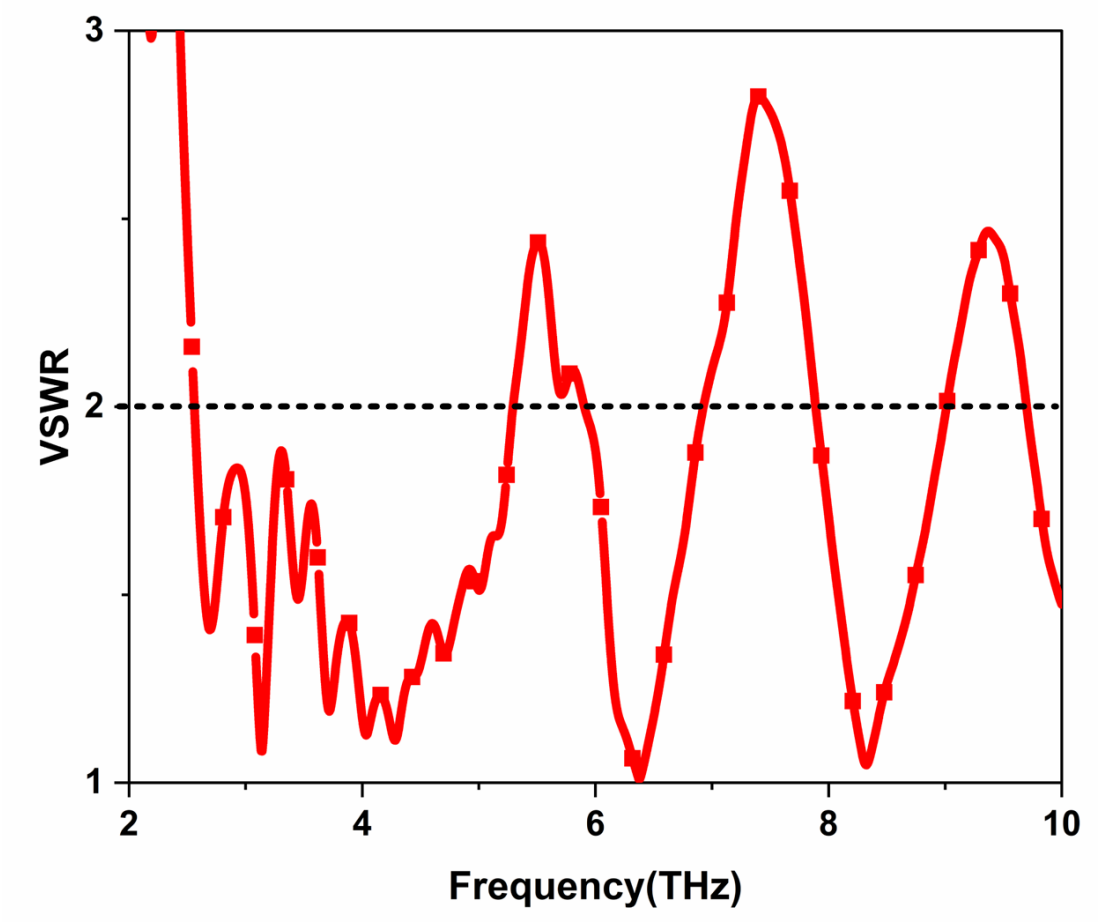

Figure 6.6: VSWR

6.2.4 Radiation Patterns

Figure 6.7 displays the copolar and crosspolar radiation patterns for both the electric field (E-field) and magnetic field (H-field) across various resonant frequencies. These patterns illustrate the propagation of electromagnetic waves in different directions relative to the antenna or radiating element. Copolar radiation patterns represent the distribution of electromagnetic energy along the same polarization axis as the transmitting antenna, while crosspolar patterns depict the energy distribution perpendicular to this axis. Analyzing these patterns at different resonant frequencies provides valuable insights into the antenna system's behavior and performance across the electromagnetic spectrum. Understanding these radiation patterns is essential for optimizing antenna designs tailored to specific applications, such as telecommunications, radar systems, or wireless networking.

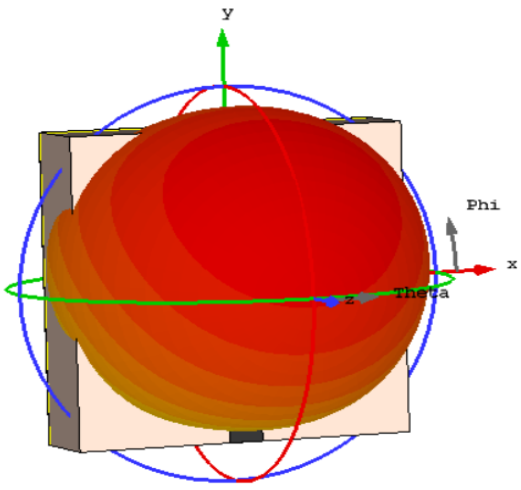

Figure 6.7: Radiation Patterns at 3.142THz

These patterns reveal the distribution of electromagnetic energy relative to the an-

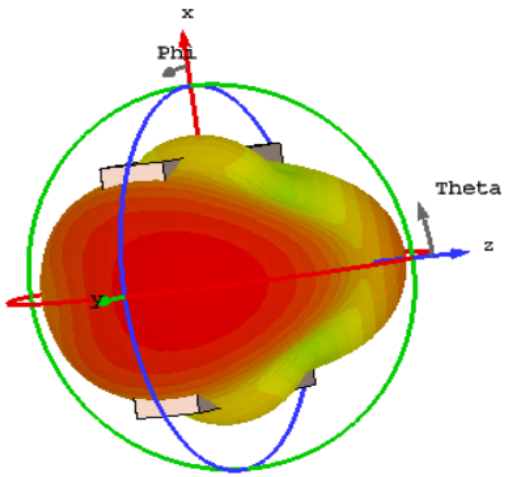

Figure 6.8: Radiation Patterns at 6.37THz

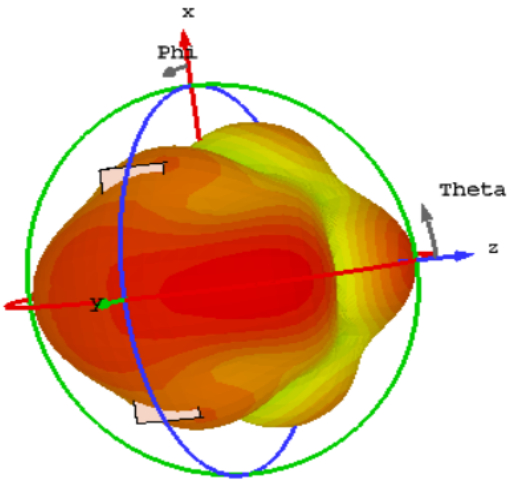

Figure 6.9: Radiation Patterns at 8.326THz

tenna's polarization axis, aiding in antenna optimization for diverse applications across the electromagnetic spectrum.

6.2.5 Surface Current

The surface current at various resonant frequencies are shown below in the Fig.6.10.

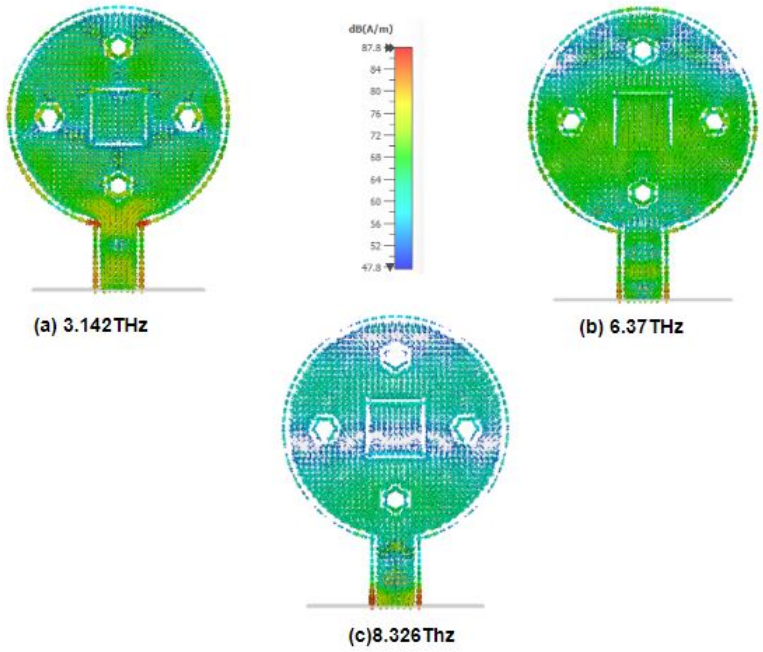

Figure 6.10: Surface Current

6.2.6 Impact of Various Materials

The antenna S11 performance at various steps of the design evolution process are shown below in the Table 6.3 that describes the impact of various antenna materials and their effects on the operating frequency bandwidths in detail.

Table 6.3: Substrate Materials and Associated Values

Substrate	**Rogers 5880**	**Polyimide**	**SiO_2**	**Quartz**
Graphene	2.90 - 3.80 4.80 - 5.90	2.57 - 5.27 5.97 - 6.88 7.91 - 8.97	2.37 - 4.70 5.75 - 6.70	2.41 - 4.83 5.82 - 7.12
Copper	5.65- 7.59 7.99-8.97	3.52 - 5.60 7.25 - 8.58	2.89 - 5.09 7.89 - 8.96	3.25 - 5.3 7.99 - 8.96
Aluminium	4.25 - 6.27 7.81 - 8.69	4.52 - 6.47 7.25 - 8.68	4.12 - 6.56 7.56 - 8.59	4.52 - 6.57 7.23 - 8.92
Gold	3.23-5.16 5.67 - 6.89	4.24 - 5.86 7.58 - 8.43	3.95 - 5.80 6.23 - 8.10	4.26 - 5.98 7.59 - 8.26

7

Conclusion & Future Scope

In this chapter, the work is concluded and future plan is presented. Next, the limitation of work and possible future extensions are described respectively.

7.1 Conclusions

Chapter 2 provides a comprehensive review of existing research, highlighting the unique features, advantages, and limitations of various approaches. This paper proposes a graphene-based patch antenna specifically designed for THz applications. The design incorporates a square ring hexagonal patch to adjust the radiation pattern and bandwidth while maintaining the operating frequency. The antenna's performance is evaluated across the 0.1–10 THz frequency range. These results demonstrate that all research objectives outlined in Sections 2.3 and 2.4 of this report have been met. A thorough parametric analysis was conducted, including the impact of various materials on antenna characteristics and the reconfigurability of graphene metamaterials. Despite its limited current use, terahertz technology holds significant promise. For its potential to be fully realized, advancements in high-performance, compact antennas are essential. The anticipated outcomes of this research are expected to significantly benefit healthcare applications.

7.2 Future Scope

Building on the proposed antenna, this work sets out several additional goals to further enhance the quality of the research. The objectives for future work include:

- Implementing Machine Learning techniques in the antenna design and optimization process to improve efficiency and resource management.
- Investigating the modifications needed to integrate MIMO technology into the proposed design.
- Exploring the inclusion of other metamaterials and analyzing their effects on antenna properties and performance.

Bibliography

[1] G. Chen, J. Pei, F. Yang, X. Y. Zhou, Z. L. Sun, and T. J. Cui, "Terahertz-wave imaging system based on backward wave oscillator," *IEEE Transactions on Terahertz Science and Technology*, vol. 2, no. 5, pp. 504–512, 2012.

[2] H. Guerboukha, K. Nallappan, Y. Cao, M. Seghilani, J. Azaña, and M. Skorobogatiy, "Planar porous components for low-loss terahertz optics," *Advanced Optical Materials*, vol. 7, no. 15, p. 1900236, 2019. [Online]. Available: https://onlinelibrary.wiley.com/doi/abs/10.1002/adom.201900236

[3] L. Chiaraviglio, A. S. Cacciapuoti, G. Di Martino, M. Fiore, M. Montesano, D. Trucchi, and N. Blefari-Melazzi, "Planning 5g networks under emf constraints: State of the art and vision," *IEEE Access*, vol. PP, 08 2018.

[4] A. Shafie, N. Yang, C. Han, J. M. Jornet, M. Juntti, and T. Kürner, "Terahertz communications for 6g and beyond wireless networks: Challenges, key advancements, and opportunities," *IEEE Network*, vol. 37, no. 3, pp. 162–169, 2023.

[5] S. Kiani, P. Rezaei, and M. Fakhr, "On-chip coronavirus shape antenna for wide band applications in terahertz band," *Journal of Optics*, vol. 52, no. 2, pp. 860–867, Jun 2023. [Online]. Available: https://doi.org/10.1007/s12596-022-01048-y

[6] Z. Xu, X. Dong, and J. Bornemann, "Design of a reconfigurable mimo system for thz communications based on graphene antennas," *Terahertz Science and Technology, IEEE Transactions on*, vol. 4, pp. 609–617, 09 2014.

[7] M. Alibakhshikenari, B. S. Virdee, S. Salekzamankhani, S. Aïssa, C. H. See, N. Soin, S. J. Fishlock, A. A. Althuwayb, R. Abd-Alhameed, I. Huynen, J. A. McLaughlin, F. Falcone, and E. Limiti, "High-isolation antenna array using siw and realized with a graphene layer for sub-terahertz wireless applications," *Scientific Reports*, vol. 11, no. 1, p. 10218, May 2021. [Online]. Available: https://doi.org/10.1038/s41598-021-87712-y

[8] M. V. Hidayat and C. Apriono, "Design of 0.312 thz microstrip linear array antenna for breast cancer imaging application," in *2018 International Conference on Signals and Systems (ICSigSys)*, 2018, pp. 224–228.

[9] S. Das, S. Ghosh, D. Samantaray, and S. Bhattacharyya, "An efficient terahertz antenna using cpw interdigital capacitor," in *2018 IEEE Indian Conference on Antennas and Propogation (InCAP)*, 2018, pp. 1–4.

[10] A. Hocini, M. Temmar, D. Khedrouche, and M. Zamani, "Novel approach for the design and analysis of a terahertz microstrip patch antenna based on photonic crystals," *Photonics and Nanostructures - Fundamentals and Applications*, vol. 36, p. 100723, 2019. [Online]. Available: https://www.sciencedirect.com/science/article/pii/S1569441019300276

[11] T. U. H. Shahid Ullah, Cunjun Ruan and X. Zhang, "High performance thz patch antenna using photonic band gap and defected ground structure," *Journal of Electromagnetic Waves and Applications*, vol. 33, no. 15, pp. 1943–1954, 2019. [Online]. Available: https://doi.org/10.1080/09205071.2019.1654929

[12] H. Zhu, X. Li, Z. Qi, and J. Xiao, "A 320 ghz octagonal shorted annular ring on-chip antenna array," *IEEE Access*, vol. 8, pp. 84 282–84 289, 2020.

[13] M. Alibakhshikenari, B. S. Virdee, C. H. See, R. A. Abd-Alhameed, F. Falcone, and E. Limiti, "High-gain metasurface in polyimide on-chip antenna based on crlh-tl for sub-terahertz integrated circuits," *Scientific Reports*, vol. 10, no. 1, p. 4298, Mar 2020. [Online]. Available: https://doi.org/10.1038/s41598-020-61099-8

[14] I. Ahmad, S. Ullah, S. Ullah, U. Habib, S. Ahmad, A. Ghaffar, M. Alibakhshikenari, S. Khan, and E. Limiti, "Design and analysis of a photonic crystal based planar antenna for thz applications," *Electronics*, vol. 10, no. 16, 2021. [Online]. Available: https://www.mdpi.com/2079-9292/10/16/1941

[15] Vishwanath, G. Varshney, and B. C. Sahana, "Design of tunable thz dielectric resonator antenna with cross-slot for circular polarization," *Optical and Quantum Electronics*, vol. 56, p. 922, 2024.

[16] R. Singh and G. Varshney, "Isolation enhancement technique in a dual-band thz mimo antenna with single radiator," *Optical and Quantum Electronics*, vol. 55, p. 539, 2023.

[17] Nishtha, R. S. Yaduvanshi, and G. Varshney, "Isolation control for implementing the single dielectric resonator based tunable thz mimo antenna and filter," *Optical and Quantum Electronics*, vol. 55, p. 357, 2023.

[18] M. F. Ali, A. Srivastava, S. Vijayvargiya, and G. Varshney, "Compact tunable terahertz self-diplexing antenna with high isolation," *Optical and Quantum Electronics*, vol. 55, pp. 1–12, 2023.

[19] A. Sivasangari, D. Deepa, P. Ajitha, R. M. Gomathi, R. Vignesh, S. K. Danasegaran, and S. Poonguzhali, "Performance analysis of metamaterial patch antenna characteristics for advanced high-speed wireless system," *Journal of Electronic Materials*, vol. 52, pp. 1234–1246, 2023.

[20] S. M. Shamim, Y. Trabelsi, N. Arafn, N. K. Anushkannan, U. S. Dina, M. A. Hossain, and N. Islam, "Design and analysis of microstrip patch antenna with photonic band gap (pbg) structure for high-speed thz application," *Optical and Quantum Electronics*, vol. 55, pp. 745–757, 2023.